Telemark University College
Faculty of technology
M.Sc. Programme

MASTER THESIS 2008

Candidate : Joachim Lundberg

Title : CFD study of a bubbling fluidized bed

Faculty of Technology
Address: Kjolnes Ring 56, N-3914 Porsgrunn, Norway, tel: +47 35 57 50 00, fax: +47 35 55 75 47
Lower Degree Programmes - M.Sc. Programmes - Ph.D. Programmes

Telemark University College

Faculty of Technology

M.Sc. Programme

WRITTEN REPORT MASTER THESIS, COURSE CODE FMH606

Student	**:**	Joachim Lundberg
Thesis Title	**:**	CFD study of a bubbling fluidized bed
Signature	**:**	. . . . .
Number of pages	**:**	82
Keywords	**:**	Drag models, Fluent 6.3, Numerical simulations, Granular properties, Richardson Zaki, Hill Koch Ladd, RUC, Syamlal O'Brien, Gidaspow, Lun et al,. . . .

Supervisor	**:** Britt Halvorsen	sign.:	. . . . .
2nd Supervisor	**:** Vidar Mathisen	sign.:	. . . . .
Sensor	**:** J. Prieur Du Plessis	sign.:	. . . . .
Sensor	**:** Sonia Woudberg	sign.:	. . . . .

External partner **:**

Availability **:** Open

Archive approval (supervisor signature): . . . . . **Date:** . . . . . .

Abstract:

The aim of this thesis is to investigate the momentum exchange between the phases in a bubbling fluidized bed. The momentum exchange can be described by a drag model. Several drag models with different assumptions are developed. The drag models investigated in this work is the Syamlal O'Brien model, the Gidaspow model, Hill Koch Ladd model, the RUC model and an iterative version of the Syamlal O'Brien called the Richardson Zaki model. The models have been derived and studied in detail.

Simulations are performed with the commercial computational fluid dynamic (CFD) code Fluent 6.3. Different models for granular material in fluidized beds are available in Fluent 6.3. The models are mostly based on the kinetic theory granular flow (KTGF). The Syamlal & O'Brien drag model and the drag model developed by Gidaspow are included in Fluent 6.3. The Hill Koch Ladd model, the RUC model and the Richardson Zaki model are implemented in Fluent by the author. Implementation of models in Fluent 6.3 is performed by using the user defined functions (UDF). The UDFs are written in C-code.

Preliminary simulations of a two dimensional fluidized bed with a central jet, are performed to investigate the effect of using turbulence models in the simulations. The laminar model gives results that agree well with experiments, and the turbulence models are not included in the further simulations.

Simulations of bubble behaviour in two and three dimensional fluidized bed with uniform inlet gas distribution are performed. Simulations in three dimensions are limited to investigate the default settings in Fluent 6.3 for two different drag models. The simulations are compared to experimental data, and the results are presented in a paper accepted for HEFAT 2008.

The main part of the simulations is done in two dimensions due to the limit of time and computational effort during this thesis. The two dimensional simulations with homogeneous air distribution in the bottom of the bed, is divided into five cases where different setups are investigated. The simulations are compared to experiments performed on a three dimensional fluidized bed, and the results agree well according to bubble frequency. It is found that a setup including multiple particle phases, free slip conditions at the walls of the bed, a second order discretization scheme for the momentum and the RUC drag model, gives the best agreement with the experimental results. This part of the thesis is presented in an abstract submitted to the SIMS 2008 conference. Further work has to be done to verify the suggested setup.

Contents

Preface

This work is based on the Doctoral thesis of Britt Halvorsen. The Interest was to investigate the effect of drag models in simulation of a bubbling fluidized beds. There was planed to do all the simulations in 3D, but this was chosen to be simplified to 2D. The reason for this was the limiting factor of time and computational effort.

One of the goals of this thesis was to implement the RUC drag model into Fluent 6.3. This model is made at the University of Stellenbosch in South Africa. This model has shown good results.

Most of the granular properties models is based on the Kinetic Theory of Granular Flow (KTGF) . This theory has been investigated and tried to describe as simple as possible. The drag models are explained in detailed in the report.

I like to thank my supervisor Britt Halvorsen for great supervising both in thesis and life and to inviting me to South Africa. Also I like to tank Professor Du Plessis and Sonia Wouldberg for taking care of us and guiding us in South Africa.

Sofiane Benyahia at the National Energy Technology Laboratory has also been very helpful to me.

At the last I like to thank Mr. Knut Vågsæther for having the ability to always have the correct answer.

Nomenclature

Latin letters

A	Constant in RUC drag model [-]
A	Constant in Syamlal O'Brien drag model [-]
A^*	Constant in Syamlal et al frictional viscosity model [Pa]
A_p	Projected area [m^2]
A_r	Archimedes number [-]
B	Constant in RUC drag model [-]
B	Constant in Syamlal O'Brien drag model [-]
C_D	Drag factor on single particle [-]
C'_D	Drag factor on multiparticle system [-]
c_i	A distance in the HKL drag model [m]
d_s	Diameter of phase s [m]
e_{ss}	restitution coefficient for phase s [-]
f	Kinetic energy loss factor in the Burke-Plummer equation [-]
F	Drag factor in HKL drag model [-]
F_{dr}	The general drag force [kg·m/s^2]
f_i	particle distribution function [-]
Fr	Friction factor from Johnson et al frictional viscosity [-]
F_0,F_1,F_2,F_3	Drag constants in the HKL drag function [-]
g	The gravitational acceleration $\left(9.81\ m/s^2\right)$ [m/s^2]
g_0	The general radial distribution function [-]
$g_{0,ss}$	The radial distribution function for phase s [-]
$\overline{\overline{I}}$	The unit tensor [-]
I_{2D}	The second invariant of the deviatoric stress tensor [-]
k	Material yield [-]
k_{Θ_s}	Conductivity of granular temperature [kg/m·s]
K_{sg}	Drag factor of phase s in phase [kg/m^3·s]
K_{sp}	Drag factor of a single particle [kg/m^3·s]
l	A length [m]
l_{mf}	Mean free path for a particle [m]
δl	A small length [m]

n	Coefficient in the Richardson and Zaki drag correlation [-]
n	Factor used in the Johnson et al frictional viscosity [-]
n_p	Number of particles or tubes [-]
n^*	Constant in Syamlal et al frictional viscosity model [-]
p	Constant from Johnson et al frictional viscosity [-]
P_s	Solids pressure [Pa]
ΔP	Pressure drop [Pa]
Q	Volumetric flow rate [m^3/s]
$\nabla \cdot q_s$	Diffusive flux of fluctuating energy [kg/m·s^3]
$\overrightarrow{r}$	Position of a lattice node in the Lattice Boltzmann theory [-]
Re	The Reynolds number [-]
Re_m	The modified Reynolds number in the Richardson Zaki correlation [-]
Re_s	The particle Reynolds number [-]
$\mathrm{Re}_{s,r}$	The particle Reynolds number based on the radius [-]
$\overline{S}_s$	Deformation rate [1/s]
t	Time [s]
Δt	Interval [s]
U	Velocity [m/s]
u_i	Phase velocity of phase i [m/s]
$u_{s,i}$ and $u_{s,j}$	Solid phase velocity in the i and j direction [m/s]
u_x	Velocity in the x direction [m/s]
v_r	The relative velocity correlation [-]
v_{sys}	Terminal settling velocity of a system of particles [m/s]
v_{sphere}	Terminal settling velocity of a sphere [m/s]
V_{tube}	Volume of a tube [m^3]
V_{solids}	Volume of solids [m^3]
w	Factor in the HKL drag correlation [-]
∂x	A small distance [m]

Greek letters

α_g	Gas phase volume fraction [-]
α_s	Solid phase volume fraction [-]
γ_{Θ_s}	Dissipation of granular temperature [kg/m·s^3]
δ	Kronecker delta [-]
Δ	Change in variable, Final-Initial [-]
η	A coefficient for simplifying [-]
∇	The Dell operator [1/m]
Θ_s	Granular temperature [m^2/s^2]
λ_s	Bulk viscosity [kg/m·s]
μ	Viscosity [kg/m·s]
μ_g	Gas viscosity [kg/m·s]
μ_s	Granular viscosity [kg/m·s]
π	The irrational number π [-]
ρ_g	Gas density [kg/m^3]
ρ_s	Solid density [kg/m^3]
$\Delta\rho$	Density difference [kg/m^3]
$\bar{\bar{\tau}}$	The stress-strain tensor [Pa]
ϕ	Angle of internal friction [$^\circ$]
ϕ	Shape factor used in the Ergun equation [-]
χ	Tortuosity [-]
χ_0	Radial distribution function for a gas [-]
Ω_i	Collision term in the Lattice boltzmann equation [-]

Subscripts

col	Collisional
dil	Dilute
fr	Frictional
g	Gas or fluid phase
int	Internal
k	Phase k used as the number k phase
kin	Kinetic
m	General solid phase m
max	Maximum
min	Minimum
pores	Pores in a porous media
q	General phase q
s	Solid phase s
st	All the solid phases.

Introduction

Fluidized beds are widely used in many industrial applications. In this work the focus will be to do simulations of experimental equipment at Telemark University College/Tel-Tek. The simulations can be used for scaling the parameters produced in the experimental equipment into industrial equipment. The main focus in this work will be to describe the bubbling frequency in the fluidized bed. This parameter describe the mixing behavior of the fluidized bed and is important when a fluidized bed with a granular catalyst is described. The economy of the process is related to how the surface of the granular catalyst is in contact with the fluid passing through. If the fluidized bed works correctly the catalytic reactions will be homogeneous in all of the reactor. If the fluidized bed works incorrect, canalization might occur and the catalyst has to be replaced before all is used.

In fluidized bed several codes are developed for simulations. This work will have focus on using a commercial CFD code. The code used is Fluent 6.3. User defined functions are used to describe the models used which is not included in the software.

Simulations will be both in 2D and 3D. The grid resolution is varied from case to case.

This work will contain the theory of some different models used to describe the properties of a granular material in a fluidized bed. The main investigations of the models used in this work is the drag models describing the momentum exchange between the phases. The drag models which are going to be used is:

- Gidaspow
- Syamlal and O'Brien
- RUC
- Hill Koch Ladd
- Richardson and Zaki (Iterative Syamlal and O'Brien)

An evaluation of which drag model who gives the bubble frequency closest to the experimental data is included.

The effect of more than one particle phase in the simulations to better describe the real data for the particles used in the experiment will be done, but the main study will be with one particle phase.

In the University of Stellenbosch a drag model called the RUC model is developed . This drag model will be implemented in Fluent 6.3 and compared with the existing drag models.

The results of this work will be used to write a paper to a conference.

Part I

Theory of multiphase modeling of bubbling fluidized bed

Chapter 1

Multiphase modeling of granular flow in Fluent 6.3

In this study the Eulerian multiphase model is used. This model will calculate one transport equation for the momentum and one for continuity for each phase. The theory for this model is taken from the reference [1].

1.1 Continuity equation

The volume fraction for each phase is calculated with an continuity equation. Equation (1.1) is a general example of the q^{th} phase volume fraction equation.

$$\frac{1}{\rho_{rq}}\left(\frac{\partial}{\partial t}\left(\alpha_q\rho_q\right)+\nabla\cdot\left(\alpha_q\rho_q\overrightarrow{u}_q\right)=\sum_{p=1}^{n}\left(\dot{m}_{sq}-\dot{m}_{sp}\right)\right) \tag{1.1}$$

Equation (1.1) is valid for both the gas phase and the solid phase. The total continuity will be all the volume fraction equations added. The ρ_{rq} is the reference density, or the volume averaged density. The right hand side of equation (1.1) is used where it is mass transfer between phases.

1.2 Gas phase momentum equation

The momentum equation for the gas is like equation (1.2).

$$\begin{aligned}\tfrac{\partial}{\partial t}\left(\alpha_g\rho_g\overrightarrow{u}_g\right)+\nabla\cdot\left(\alpha_g\rho_g\overrightarrow{u}_g\overrightarrow{u}_g\right)= \quad & -\alpha_g\nabla p+\nabla\cdot\overline{\overline{\tau}}_g+\alpha_g\rho_g\overrightarrow{g}\\ & +\textstyle\sum_{p=1}^{n}\left(K_{pg}\left(\overrightarrow{u}_p-\overrightarrow{u}_g\right)+\dot{m}_{pg}\overrightarrow{u}_{pg}-\dot{m}_{gp}\overrightarrow{u}_{gp}\right)\\ & +\left(\overrightarrow{F}_g+\overrightarrow{F}_{lift,g}+\overrightarrow{F}_{vm,g}\right)\end{aligned} \tag{1.2}$$

Equation (1.2) can be simplified to a simpler expression when assuming no mass transfer between the phases and no lift and virtual mass force. The simplified expression will be like equation (1.3).

$$\frac{\partial}{\partial t}\left(\alpha_g \rho_g \overrightarrow{u}_g\right) + \nabla \cdot \left(\alpha_g \rho_g \overrightarrow{u}_g \overrightarrow{u}_g\right) = -\alpha_g \nabla P + \nabla \cdot \overline{\overline{\tau}}_g + \alpha_g \rho_g \overrightarrow{g} + K_{sg}\left(\overrightarrow{u}_s - \overrightarrow{u}_g\right) \tag{1.3}$$

The $\overline{\tau}_g$ is the gas phase stress-strain tensor is shown in equation (1.4).

$$\overline{\overline{\tau}}_g = \alpha_g \mu_g \left(\nabla \overrightarrow{u}_g + \nabla \overrightarrow{u}_q^T\right) + \alpha_g \left(\lambda_q + \frac{2}{3}\mu_g\right) \nabla \cdot \overrightarrow{u}_g \overline{\overline{I}} \tag{1.4}$$

1.3 Granular phase momentum equation

The assumptions for the granular phase equation (1.5) is the same as for the gas phase.

$$\frac{\partial}{\partial t}\left(\alpha_s \rho_s \overrightarrow{u}_s\right) + \nabla \cdot \left(\alpha_s \rho_s \overrightarrow{u}_s \overrightarrow{u}_s\right) = -\alpha_s \nabla P + \nabla \cdot \overline{\tau}_s + \nabla P_s + \alpha_s \rho_s \overrightarrow{g} + K_{gs}\left(\overrightarrow{u}_g - \overrightarrow{u}_s\right) \tag{1.5}$$

The momentum equation for gas and granular phase is quite similar except for the granular pressure in the granular phase. Here the stress-strain tensor $\overline{\overline{\tau}}_s$ is like equation (1.6).

$$\overline{\overline{\tau}}_s = \alpha_s \mu_s \left(\nabla \overrightarrow{u}_s + \nabla \overrightarrow{u}_s^T\right) + \alpha_s \left(\lambda_s + \frac{2}{3}\mu_s\right) \nabla \cdot \overrightarrow{u}_s \overline{\overline{I}} \tag{1.6}$$

Chapter 2

Theory of properties models in Fluent 6.3

To describe the behavior of the granular material in a fluidized bed the properties needs to be defined. The granular phase is defined by property models for the interactions with other particles and fluid phases.

2.1 Granular viscosity

In Fluent 6.3 the granular viscosity is a summation of three viscosity contributions. The collisional, kinetic and frictional viscosities is combined in equation (2.1).

$$\mu_s = \mu_{s,\text{col}} + \mu_{s,kin} + \mu_{s,fr} \tag{2.1}$$

The collisional viscosity is a viscosity contribution due to collisions between particles is taken from the kinetic theory of granular flow of Lun et al [2]. The collisional viscosity contribution is shown in equation (2.2).

$$\mu_{s,\text{col}} = \frac{4}{5}\alpha_s \rho_s g_{0,ss} (1 + e_{ss}) \sqrt{\frac{\Theta_s}{\pi}} \tag{2.2}$$

In equation (2.2), $g_{0,ss}$ is the radial distribution function and is explained in chapter 2.7, Θ_s is the granular temperature and is explained in chapter 3 and e_{ss} is the restitution coefficient and is explained in chapter 3.6.

In the granular viscosity option in Fluent 6.3 it is possible to choose two models for the kinetic viscosity, either (2.4) or (2.7). Fluent 6.3 calculate the frictional viscosity but this is defined in another option. The contribution from the different viscosities vary in different regimes. In the dilute regime the probability of particle collisions is low, and the largest contribution in dilute regimes is the kinetic viscosity. In very dense particle regimes the frictional viscosity has the largest contribution. The very dense region will be close to the maximum packing limit. In between the dense and dilute regimes its the viscous regime.The particles will move like a fluid, but the probability of particle collisions is large. Since the particles have a high probability of collisions they will most probably not get a high speed. This means that the kinetic contribution will be very small. The particles will not get a high speed cause they collide

all the time. The collisional viscosity will have the highest contribution in the viscous regime.

2.1.1 Syamlal et al

The model for kinetic viscosity by Syamlal et al shown in equation (2.3) is based on the modified kinetic theory for smooth, inelastic spherical particles by Lun et al [2]. This model assumes that the kinetic contribution to the viscosity is neglectable in the dilute region. [3]

$$\mu_{s,kin} = \frac{\alpha_s d_s \rho_s \sqrt{\Theta_s \pi}}{6\left(3 - e_{ss}\right)} \left[1 + \frac{2}{3}\left(1 + e_{ss}\right)\left(3e_{ss} - 1\right)\alpha_s g_{0,ss}\right] \tag{2.3}$$

2.1.2 Gidaspow et al

The theory of the Gidaspow et al model for the collisional viscosity is taken from the reference [4].

The model of kinetic viscosity by Gidaspow et al (2.4) is a extension of the kinetic theory in the reference [5, 6].

$$\mu_{kin} = \frac{2\mu_{dil}}{\left(1 + e_{ss}\right) g_{0,ss}} \left[1 + \frac{4}{5} g_{0,ss} \alpha_s \left(1 + e_{ss}\right)\right]^2 \tag{2.4}$$

The model is based on the dilute viscosity of a gas and is taken from the kinetic theory of gasses. It assumed that a molecule is hard spherical particle. It is also assumed that the particles in the dilute region like a molecule in low pressures do not collide. The restitution coefficient equal 1 and the radial distribution function equal 1. This will make the dilute viscosity a function like equation (2.5).

$$\mu_{dil} = (\text{constant}) * (\text{bulk density }) * (\text{mean free path}) * (\text{oscillation velocity}) \tag{2.5}$$

According to the reference [4] the constant equal $\frac{5\sqrt{\pi}}{96}$ the particle bulk density for dilute regimes is $\rho_{dil} = \rho_s \alpha_s$ the mean free path is $l_{mf} = \left(\frac{d_s}{\alpha_s}\right)$ and the oscillating velocity is $\sqrt{\Theta}$. When multiplying this factors the expression for the dilute viscosity is (2.6).

$$\mu_{dil} = \frac{5\sqrt{\pi}}{96} \left(\rho_s \alpha_s\right) \left(\frac{d_s}{\alpha_s}\right) \sqrt{\Theta} \tag{2.6}$$

In Fluent 6.3 the kinetic viscosity is volume averaged which means $\mu_{kin} = \mu_{s,kin}\alpha_s$. By inserting this equation (2.6) into the extensions of the kinetic theory [5, 6] which is corrected for large volume fractions of particles and non unity restitution coefficients the expression for the kinetic viscosity becomes (2.7).

$$\mu_{s,kin} = \frac{10\rho_s d_s \sqrt{\Theta_s \pi}}{96\alpha_s \left(1 + e_{ss}\right) g_{0,ss}} \left[1 + \frac{4}{5} g_{0,ss} \alpha_s \left(1 + e_{ss}\right)\right]^2 \tag{2.7}$$

If the volume fraction of the solid material approaches zero, and the restitution coefficient approaches one, the kinetic viscosity will be equal the dilute viscosity.

2.2 Granular bulk viscosity

The granular bulk viscosity is the resistance the granular particles have to compression or expansion. The model is developed from the kinetic theory of granular flow and is taken from Lun et al [2]. This model is like the equation (2.8).

$$\lambda_s = \frac{4}{3}\alpha_s \rho_s d_s (1 + e_{ss}) \sqrt{\frac{\Theta_s}{\pi}} \tag{2.8}$$

2.3 Frictional viscosity

The frictional viscosity is the contribution of the friction between particles to the total shear viscosity. When the solids volume fraction α_s gets close to the maximal packing limit $\alpha_{s,\max}$ the particles get very close to each other. The main stress will be due to friction and rubbing between the particles.

According to the reference [7] the stresses in the frictional regime is described by the a phenomena rather than the mechanistic models describing the viscous regime. The theory for the frictional pressure is adopted from the soil mechanics. This theories is a combination of a yield function and a flow rule. The yield function is the function of the stress tensor for a material about to yield. An example of this can be if a sand castle is build upon a horizontal plate, and one side of it is lifted. The stress tensor describing the moment right before it will break and fall down on the opposite side of where it is lifted is the yield function for the system. The flow rule is a set of relations between the components of the stress and the rate of strain.

In Fluent 6.3 it has to be defined a limit for the frictional viscosity. This limit is the volume fraction of solids α_s reach a chosen value where the frictional regime starts to get important. At this limit the calculation of the frictional viscosity will begin The frictional viscosity will not contribute in the viscous or dilute regimes. And of this reason this so called "switch" is made to turn of and on the frictional viscosity calculation. This calculations of the frictional viscosity takes lots of computational effort to calculate. Of this reason a limit for the frictional stress calculations is made [3]. Fluent 6.3 has an option to disable the calculation of the frictional viscosity completely even in the high fractions of solids [1]. In Fluent 6.3 has two models for the frictional viscosity.

2.3.1 Schaeffer

The Schaeffer expression for the frictional viscosity is shown in equation (2.9).

$$\mu_{s,fr} = \frac{P_{s,fr} \sin\phi}{2\sqrt{I_{2D}}} \tag{2.9}$$

In equation (2.9) $P_{s,fr}$ is the frictional pressure. The constant ϕ, is the angel of internal friction. The I_{2D} is the second invariant of the deviatoric stress tensor [1]. When the angle of internal friction goes to zero, the frictional viscosity will converge zero.

The second invariant of the deviatoric stress tensor can be written as (2.10).

$$I_{2D} = \frac{1}{6}\left[(D_{s11} - D_{s22})^2 + (D_{s22} - D_{s33})^2 + (D_{s33} - D_{s11})^2\right] + D_{s12}^2 + D_{s23}^2 + D_{s31}^2 \tag{2.10}$$

The $D_{s...}$ from equation (2.10) can be written in the general form showed in equation (2.11).

$$D_{s,ij} = \frac{1}{2}\left(\frac{\partial u_{s,i}}{\partial x_j} + \frac{\partial u_{s,j}}{\partial x_i}\right) \tag{2.11}$$

If the stress tensor is considered and the hydrostatic pressure is subtracted from it the stresses governing volumetric deformation is left. This gives three invariants of the stress tensor. The first invariant is the hydrostatic stress or pressure. The second invariant is related to the shear stresses. The third express the deformation behavior of a formed part. [8, 9] In the von Mises yield criteria it says at it is a correlation between the second invariant of the stress tensor and a constant k. This constant k is where the material yield. According to Schaeffer [10] the constant k equals $\sin(\phi)$ where ϕ is the angle of internal friction.

Drucker and Prager were the first to propose a principle of plastic flow to granular flow [11]. They proposed a balance between the hydrostatic pressure and the square of the second invariant of the deviatoric stress tensor. By combining this with a flow rule Schaeffer made the model for the frictional viscosity.

2.3.2 Johnson et al.

In the model from [11] for the frictional viscosity it is proposed a model that relates the normal forces to the shear forces. The model is for fully developed plane shear of a non-cohesive material. It is assumed that the critical state and the shear stresses is proportional to the normal stress. The theories for this model is in equation (2.12) are based on a empirical values cause the problem is in nature very complicated and is dependent on quantities not directly on particle diameter or roughness of the particles.

The model for frictional viscosity from [11] is based on the Coulombs law [11] and is shown in equation (2.12).

$$\mu_{s,fr} = P_{s,fr}\sin(\phi) \tag{2.12}$$

The angle of internal friction, ϕ, is in the reference [11] set to $28.5\,^\circ$.

2.4 Frictional pressure

The frictional pressure is the pressure modeled when the particles is so close that the particles will be in contact all the time. The random motion in the particles will be minimal. The particles will move very slow compared to the viscous regime. In the frictional or plastic regime the pressure will get higher than in the other regimes cause here the particles have very little place to move.

The stresses due to contact between particles is calculated separately from the pressure due to collisions and kinetics (solids pressure explained in chapter 2.6).

In Fluent 6.3 three models for the frictional pressure is included.

2.4.1 Johnson et al

The model Johnson et al for the frictional pressure (2.13) is experimental based. In the [12] they claim that the description of the quasi static behavior of a granular flow in a dense region is in nature mostly empirical. This require lots of experimental data to describe any material to find the correct behavior in the dense or frictional regime. The model from Johnson et al is for a "dry" cohesionless particulate flow, which means that no fluid is surrounding the particles and they will not stick to each other. Experimental observations show that the pressure will increase rapidly with increasing volume fraction in the dense region, like when liquid is compressed. Johnson et al make a simple algebraic expression for the solids pressure in the frictional region.

$$P_{s,fr} = Fr\frac{(\alpha_s - \alpha_{s,\min})^n}{(\alpha_{s,\max} - \alpha_s)^p} \tag{2.13}$$

Where Fr, $\alpha_{s,\min}$, n and p is experimental based parameters. In the reference [11] the parameters proposed for Fr, $\alpha_{s,\min}$, n and p is 3.65 e^{-32} ,0.5, 0 and 40. In later work by the reference [12] the parameters where corrected to 0.05, 0.5, 2, and 5. The $\alpha_{s,\min}$ is the frictional limit where the frictional particle interactions start to occur. This parameters is made for spherical glass particles with the diameter of 1mm and the density $\rho_s = 2900\ kg/m^3$. The parameters used in Fluent 6.3 is Fr, $\alpha_{s,\min}$, n and p and are modified by [13] to 0.05, 0.5, 2, 3. Fluent 6.3 uses this modification but $\alpha_{s,\min}$ is possible to set in user interface. The default value for $\alpha_{s,\min}$ is 0.61. Fluent have also modified the parameter Fr to be a function of α_s which is shown in equation (2.14).

$$Fr = 0.1\alpha_s \tag{2.14}$$

2.4.2 Syamlal et al

The model for the frictional pressure from Syamlal et al is a typical power law which starts at the frictional packing limit. This model has the form like in equation (2.15).

$$P_{s,fr} = A^* \left(\alpha_s - \alpha_{\min,fr}\right)^{n^*} \tag{2.15}$$

Where the constants A^* and n^* is 10^{25} and 10.

2.4.3 Based-KTGF

The based-KTGF uses the kinetic theory of granular flow. This theory includes the radial distribution function and the granular temperature. The radial distribution will go to infinity as the solids volume fraction goes to the maximal packing limit. This can be coupled to the solids pressure by a solids pressure model. In the based-KTGF model the frictional pressure equals the solids pressure. This model is the default model for frictional pressure in Fluent 6.3. [1]

The based-KTGF model is not appropriate for the Syamlal O'Brien radial distribution function explained in chapter 2.7.2 because this model do not have a asymptotic behavior at high volume fractions of particles.

2.5 Granular conductivity

The granular conductivity describes the diffusive flux of granular energy or granular temperature. The default model in Fluent 6.3 is the model by Syamlal et al, but a model by Gidaspow is also available.

2.5.1 Syamlal et al

The model for the granular conductivity by Syamlal et al shown in equation (2.16) is taken from Lun et al's kinetic theory of granular flow [3]. The model is a modification of the granular conductivity of a perfectly elastic particle, to take into account inelastic collisions between particles when the restitution coefficient is less than one ($e_{ss} < 1$) [2].

The model is shown in equation (2.16).

$$k_{\Theta_s} = \frac{15 d_s \rho_s \alpha_s \sqrt{\Theta_s \pi}}{4\left(41 - 33\eta\right)} \left[1 + \frac{12}{5}\eta^2 \left(4\eta - 3\right) \alpha_s g_{0,ss} + \frac{16}{15\pi}\left(41 - 33\eta\right)\eta \alpha_s g_{0,ss}\right] \tag{2.16}$$

2.5.2 Gidaspow

The other option in Fluent 6.3 is the model for granular conductivity by Gidaspow shown in equation (2.17). This is based on kinetic gas theory and modified to particle flow [4].

The model by Gidaspow is shown in equation (2.17).

$$k_{\Theta_s} = \frac{150 \rho_s d_s \sqrt{\Theta \pi}}{384\left(1 + e_{ss}\right) g_{0,ss}} \left[1 + \frac{6}{5}\alpha_g g_{0,ss}\left(1 + e_{ss}\right)\right]^2 + 2\rho_s \alpha_s^2 d_s \left(1 + e_{ss}\right) g_{0,ss} \sqrt{\frac{\Theta_s}{\pi}} \tag{2.17}$$

This model differs significant from the model by Syamlal et al shown in equation (2.16) at restitution coefficients significant different from one.

2.6 Solids pressure

In regions where the particle volume fraction α_s is lower than the maximum allowed fraction $\alpha_{s,\max}$, the solids pressure is calculated independently and used in the pressure gradient term ∇p_s. The solid pressure is composed of a kinetic term and a term due to particle collisions. [1] In dense regions of the fluidized bed the collisional term is the most dominant. [14] Experiments by Campell and Wang [14] show that the solids pressure is highest when the fluidized bed is not fluidized. It will decrease until the minimum fluidization is engaged. When the gas velocity is further increased the solids pressure is also increased due to particle collisions. [14]

Fluent 6.3 has three models for calculating the solid pressure.

2.6.1 Lun et al

The Lun et al model shown in equation (2.18) compensate for both kinetic and the collisional contribution. It is derived from the kinetic theory of granular flow. [2]

$$p_s = \alpha_s \rho_s \Theta_s + 2\rho_s (1 + e_{ss}) \alpha_s^2 g_{0,ss} \Theta_s \tag{2.18}$$

2.6.2 Syamlal O'Brien

The Syamlal O'Brien model for solids pressure shown in equation (2.19), is almost the same as the Lun et al model (2.18) except that the Syamlal O'Brien model neglect the solids pressure produced by the kinetic term.

$$p_s = 2\rho_s (1 + e_{ss}) \alpha_s^2 g_{0,ss} \Theta_s \tag{2.19}$$

2.6.3 Ma Ahmadi

The Ma Ahmadi for solids pressure (2.20) is some what similar to the Lun et al model shown in equation (2.18) but it takes in account the frictional viscosity which is explained in chapter 2.3. The model is derived using turbulence theory from a modified k-ε turbulence model. The Ma Ahmadi model for solids pressure should be used together with the Ma Ahmadi model for radial distribution function which is explained in chapter 2.7.3. [1]

$$p_s = \alpha_s \rho_s \Theta_s \left[(1 + 4\alpha_s g_{0,ss}) + \frac{1}{2} \left[(1 + e_{ss}) \left(1 - e_{ss} + 2\mu_{fric} \right) \right] \right] \tag{2.20}$$

2.7 Radial distribution function

The radial distribution function g_0 is a function that modify the probability of collisions between particles. It can be described as equation (2.21). [1]

$$g_0 = \frac{l + d_p}{l} \tag{2.21}$$

In this function (2.21), d_p is the particle diameter and l is the length between the particles. When the particles are very close the length l goes to zero and the radial distribution function, g_0, goes to infinity. Then no motion is possible. This is the case when the packing of the particles is very dense. In a dilute solution the particles have a very low volume fraction and then the probability of collisions are very low. In such a case the distance between the particles is large, and the radial distribution function g_0 will go to one. This theory is closely linked to the gas theory [1]. In the gas theory by the reference [15] the radial distribution is χ_0. This function can be transformed into a function only depending the solid phase volume fraction α_s. The expression for the radial distribution is as in equation (2.22).

$$\chi_0 = 1 + \frac{5}{2}\alpha_s + 4.5904\alpha_s^2 \tag{2.22}$$

In the granular theory the radial distribution is modified from the χ_0 to g_0 and the expression is in general like equation (2.23). This equation was first given by Ogawa et al [16].

$$g_0 = \left[1 - \left(\frac{\alpha_s}{\alpha_{s,\max}} \right)^{\frac{1}{3}} \right]^{-1} \tag{2.23}$$

The comparison between the models is shown in Figure 2.1. It is assumed that the $\alpha_{s,\max} = 0.63$.

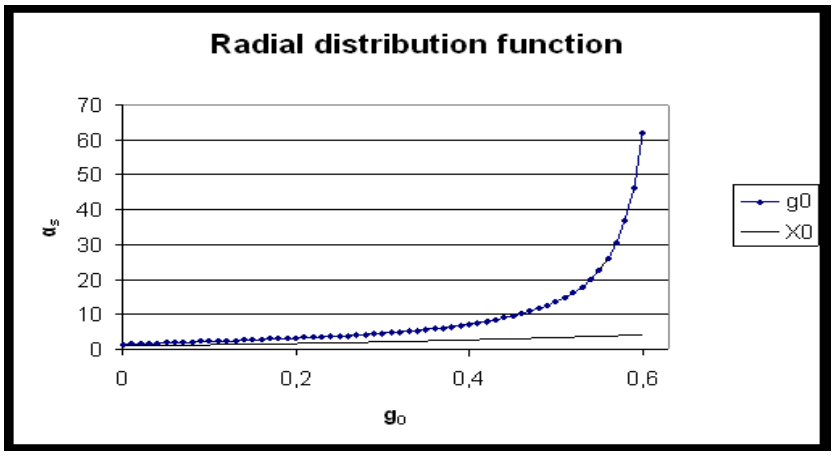

Figure 2.1: Radial distribution from granular theory and gas theory

Equation (2.23) takes only in account one particle phase. To take this into account Fluent 6.3 has four different models for the radial distribution function for more than one particle phase [1]. The g_0 is also modified when the number of solid phases is greater than one as in equation (2.24).

$$g_{0,sm} = \frac{d_m g_{0,ss} + d_l g_{0,mm}}{d_m + d_s} \tag{2.24}$$

This means that it takes into account the direct effect of solid phase s on solid phase m and also the indirect effect from l on all the other solid phases.

2.7.1 Lun et al

The Lun et al model for the radial distribution showed in equation (2.25) is quite similar to the general form given by Ogawa et al in equation (2.23) [16] but it have an extra therm who takes into account more than one particle phase.

$$g_{0,ss} = \left[1 - \left(\frac{\alpha_{st}}{\alpha_{st,\max}}\right)^{\frac{1}{3}}\right]^{-1} + \frac{1}{2} d_s \sum_{k=1}^{N} \frac{\alpha_k}{d_k} \tag{2.25}$$

In equation (2.25) index st denotes the sum of all the particle phases. The index s is the s-th solid phase and k is all the solid phases (2.26).

$$\alpha_{st} = \sum_{k=1}^{N} \alpha_k \tag{2.26}$$

If the number of solid phases equals one, equation (2.25) will be reduced to the proposed model by Ogawa et al shown in equation (2.23).

2.7.2 Syamlal O'Brien

The model by Syamlal and O'Brien (2.27) was derived by Lebowitz [17] and is for a mixture of hard spheres [3].

$$g_{0,ss} = \frac{1}{(1-\alpha_s)} + \frac{3\left(\sum_{k=1}^{N} \frac{\alpha_k}{d_k}\right)}{(1-\alpha_s)^2 (d_l + d_k)} d_k d_l \tag{2.27}$$

Here (2.27) the effect of other solid phases is included in the model.

2.7.3 Ma Ahmadi

The model for the radial distribution function by Ma Ahmadi (2.28) is based on the turbulent kinetic energy in the solid phase. The model is derived from a modified version of the k-ε model. This model takes into account the crowding effect and is given for a $\alpha_{s,\max} = 0.64356$. [18]

$$g_{0,ss} = \frac{1 + 2.5\alpha_s + 4.5904\alpha_s^2 + 4.515439\alpha_s^3}{\left[1 - \left(\frac{\alpha_s}{\alpha_{s,\max}}\right)^3\right]^{0.678021}} + \frac{1}{2} d_s \sum_{k=1}^{N} \frac{\alpha_k}{d_k} \tag{2.28}$$

2.7.4 Arastoopour

The model for radial distribution by Arastoopour [19] is shown in equation (2.29).

$$g_{0,ss} = \frac{1}{\left(1 - \frac{\alpha_s}{\alpha_{s,\max}}\right)} + \frac{3}{2} d_s \sum_{k=1}^{N} \frac{\alpha_k}{d_k} \tag{2.29}$$

This model (2.29) is some what similar to the model by Syamlal O'Brien in equation (2.27), but it differs in the high solids fractions. This model fits better with the data from the molecular dynamic simulator by Alder and Wainwright. [20]

2.7.5 Comparing the different models for radial distribution in Fluent 6.3

A study of the different radial distribution functions is performed. The result is shown in Figure 2.2 where $\alpha_{s,\max} = 0.64356$ and the diameter of the solid phase is set to 490 μm.

This Figure 2.2 show that the Ogawa et al (2.23) and the Lun et al (2.25) gives similar results, which is reasonable. They also give a high probability for collisions at high concentrations. The Ma Ahmadi model in equation (2.28) and the Arastoopour model in equation (2.29) give a quite similar results which seems reasonable in comparing with data from [20]. The Syamlal O'Brien model in equation (2.27) seems to under predict the probability of collisions.

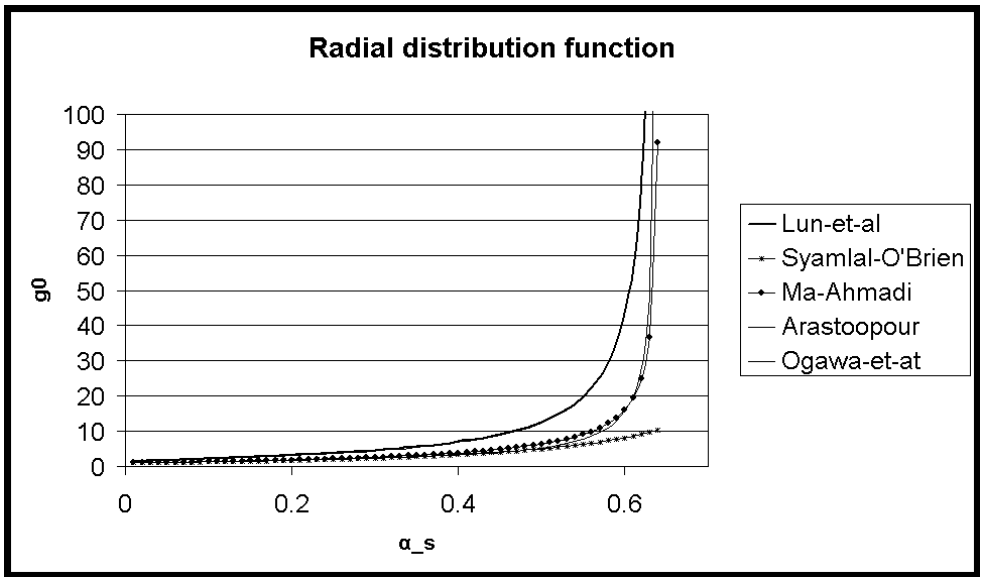

Figure 2.2: Comparison of all the radial distribution functions in Fluent 6.3

Chapter 3

Granular temperature

The granular temperature is a measurement of the random motion in particles. It is proportional to the mean square of the random motion of particles. Due to mechanical energy transferred to the granular particles generation of random motion in the particles is made. This motion will further make internal energy in the particles. [1, 4] An example is if two particles collide. If the collision is a perfect inelactic collision, all the kinetic energy is conserved. In one dimension this means that the velocity of the particles will be the same before and after the coalition, but in the opposite direction. In real life the coalition is not perfect and some of the particle will have a increase in thermal temperature. If more particles are included and in two and tree dimensions, the motion of the particles will start to get random. The measurement of this motion is called granular temperature.

It is an option in Fluent 6.3 if the granular temperature shall be solved as a partial differential equation or a algebraic expression. In the algebraic expression the diffusion and the convection is neglected. [1]

3.1 Transport equation for granular temperature

The transport equation for granular temperature Θ for solid phase s, can be written as equation (3.1) [6]

$$\frac{3}{2}\left[\frac{\partial}{\partial t}\left(\rho_s \alpha_s \Theta_s\right) + \nabla \cdot \left(\rho_s \alpha_s \overrightarrow{u}_s \Theta_s\right)\right] = \overline{\overline{\tau}}_s : \nabla \overrightarrow{u}_s - \nabla \cdot q_s - \gamma_{\Theta_s} - 3K_{sg}\Theta_s \quad (3.1)$$

In words this equation (3.1) can be explained as equation (3.2).

$$\begin{aligned} \text{Transient term + Convective term} = \quad & \text{Solid phase stress -Flux of fluctuating energy} \\ & \text{- Collisional energy dissipation} \\ & \text{+ Exchange term with phase } g \end{aligned} \quad (3.2)$$

The right hand side of the transport equation for granular temperature is further explained in the following chapters. All the definitions are taken from the reference [6]

3.2 Solid phase stress

The generation of granular temperature is due to solid stresses.

$\overline{\overline{\tau}}_s$ is the solid phase stress and can be written as equation (3.3).

$$\overline{\overline{\tau}}_s = [-P_s + \alpha_s \lambda_s \nabla \cdot \overrightarrow{u}_s] \overline{\overline{I}} - 2\alpha_s \mu_s \overline{S}_s \tag{3.3}$$

In equation (3.3), p_s is the solid pressure and is explained in chapter 2.6, λ_s is the granular bulk viscosity and is explained in chapter 2.2, $\overline{I}$ is the unit tensor, μ_s is the granular viscosity and is explained in chapter 2.1 and $\overline{S}_s$ is the deformation rate and is written as equation (3.4).

$$\overline{S}_s = \frac{1}{2}\left[\nabla \overrightarrow{u}_s + (\nabla \overrightarrow{u}_s)^T\right] - \frac{1}{3}\nabla \cdot \overrightarrow{u}_s \overline{I} \tag{3.4}$$

3.3 Flux of fluctuating energy

The $\nabla \cdot q_s$ term describe the diffusive flux of fluctuating or granular energy. [1] q_s can be written as equation (3.5).

$$q_s = k_{\Theta_s} \nabla \Theta_s \tag{3.5}$$

k_{Θ_s} is the granular conductivity of granular temperature. This coefficient is further explained in th chapter 2.5.

3.4 Collisional energy dissipation

γ_{Θ_s} is the dissipation of granular temperature. Due to collisions between particles in the phase s, the energy in the particles will dissipate. The algebraic equation for collisional energy dissipation is derived by Lun et al [2] and showed in equation (3.6).

$$\gamma_{\Theta_s} = \frac{12\left(1 - e_{ss}^2\right) g_{0,ss}}{d_s \sqrt{\pi}} \rho_s \alpha_s^2 \sqrt{\Theta_s^3} \tag{3.6}$$

When the restitution factor e goes to 1, the dissipation of the granular temperature goes to zero. This means that the particles are perfectly elastic. [2]

3.5 Exchange term with phase g

The exchange coefficient K_{sg} is the drag factor of the particles. This is further explained in chapter 4.

3.6 Restitution coefficient

The restitution coefficient e_{ss} specify the the coefficient of restitution for collisions between particles. The coefficient e_{ss} is for the collisions between particles of the solid phase s. It is also possible to specify the coefficient of restitution between the solid phase s and other particle phases. [1]

The restitution coefficient compensate for the collisions to be inelastic. In a completely elastic collision the restitution coefficient will be one. In a collision between particles some "heat" will be generated. This "heat" will be the granular temperature.

Further investigation of the parameter e_{ss} has not been done and the default restitution coefficient from Fluent 6.3 has been used. This coefficient is 0.9.

Chapter 4

Drag models

To describe the momentum exchange between phases drag models are made. The drag models available in Fluent 6.3 suited for a fluidized bed simulation is the Gidaspow model and the Syamlal O'Brien model. Both are derived in the following chapters. Some new models are also investigated.

4.1 Syamlal O'Brien

The drag model of Madhava Syamlal and Tomas O'Brien is a correlation between the drag of a sphere and a multiparticle system. The model is shown in equation (4.1).

$$K_{sg} = \frac{3\alpha_g \alpha_s \rho_g}{4 d_s v_r^2} C_D \left| \overrightarrow{u_s} - \overrightarrow{u_g} \right| \tag{4.1}$$

The derivation of this model start with the drag model for a uniform sphere. This can be derived from the dynamic pressure $P_{dyn} = \frac{1}{2}\rho u^2$. Where the dynamic pressure is a force per a area. The dynamic pressure is multiplied by a drag factor C_D resulting in a drag force shown in like equation (4.2).

$$F_{dr} = \frac{1}{2}\rho_g C_D U^2 A_p \tag{4.2}$$

This expression (4.2) is the total drag force but it is choose to have it on the form $F_{dr} = K_{sg} U$ where U is the interracial velocity difference.

$$F_{dr} = K_{sg} \left(\overrightarrow{u_s} - \overrightarrow{u_g} \right) \tag{4.3}$$

By using this (4.3) the drag model K_{sg} is made.

For a volume the number of equally sized particles per volume n_p will be (4.4).

$$n_p = \frac{6\left(1-\alpha_g\right)}{\pi d_p^3} \tag{4.4}$$

The next thing to do is to multiply the drag model for one particle with the number of particles per volume shown in equation(4.5).

$$K_{sg} = \frac{1}{2}\rho_g C_D U A \frac{6\left(1-\alpha_g\right)}{\pi d_p^3} \tag{4.5}$$

The area used in the drag factor A_p is the projected frontal area of the particle. And here it is used the superficial velocity $U = \alpha_g \left|\overrightarrow{u_s} - \overrightarrow{u_g}\right|$. Then inserting this into the equation (4.5) to make the expression (4.6).

$$K_{sg} = \frac{3\rho_g \alpha_g \left(1 - \alpha_g\right)}{4d_p} C_D \left|\overrightarrow{u_s} - \overrightarrow{u_g}\right| \tag{4.6}$$

The model shown in equation (4.6) is the drag for all the particles in the volume acting alone, but in a fluidized bed they will act as a multiparticle system. To find this model, the drag factor C_D can be modified to a drag factor C_D' for a multiparticle system.

To find this a dimensional analyses of both the scenario with single particles and the multiparticle case is performed. The single particle may be written as equation (4.7).

$$f\left(\rho_g, \Delta\rho, g, \mu_g, l\right) \tag{4.7}$$

This means that the system is a function of the fluid density, ρ_g, the density difference of the fluid and the particles, $\Delta\rho$, the gravitational forces, g, the viscosity of the fluid surrounding the particles, μ_g and a length scale. The dimensions of the properties are

$$\begin{aligned} \rho_g &= L^{-3}M \\ \Delta\rho &= L^{-3}M \\ g &= MT^{-2} \\ \mu_g &= ML^{-1}T^{-1} \\ l &= L \end{aligned}$$

Where L is a length, M is a mass and T is a time. By multiplying all the properties and rise them to the power of $[a, b, c, d, e]$ we get the expression shown in equation (4.8).

$$\left(\rho_g\right)^a \left(\Delta\rho\right)^b \left(g\right)^c \left(\mu_g\right)^d \left(l\right)^e \tag{4.8}$$

The matrix for the dimensions will be

$$\begin{array}{c|ccccc} & a & b & c & d & e \\ L & -3 & -3 & 1 & -1 & 1 \\ M & 1 & 1 & 0 & 1 & 0 \\ T & 0 & 0 & -2 & -1 & 0 \end{array} = \begin{array}{c} r \\ -5 \\ 3 \\ -3 \end{array}$$

By solving this matrix to get the dimensions correct (all the numbers in the r-column =0) it is found that $d = -2$ and $e = 3$. This will give the dimensionless size shown in equation (4.9).

$$\frac{\rho_g \Delta\rho g l^3}{\mu_g^2} \tag{4.9}$$

The characteristic length scale of this system is the particle diameter and $\Delta\rho = \left(\rho_g - \rho_s\right)$ This dimensionless size can be found in the literature to be the Archimedes number shown in equation (4.10) and relates the gravitational forces to the viscous forces.

$$Ar = \frac{\rho_g \left(\rho_g - \rho_s\right) g d_s^3}{\mu_g^2} \tag{4.10}$$

When the multiparticle system is considered and it is assumed that it is no solid stress [4]. In The drag model by Syamlal O'Brien, this is assumed [21]. In this case the Archimedes number is the same for a single particle system and a multiparticle system. Then with that assumption the drag factor C_D in the single particle can be related to the multiparticle drag factor C'_D. This can be done by doing a dimension analyses of the drag factor C_D and C'_D. This is done in the reference [21]. The result found is $C_D = f(\mathrm{Re})$ and $C'_D = f(\mathrm{Re}_s, \alpha_g)$. Under terminal settling conditions the drag forces will equal the gravitational force minus the buoyant force of the particle. this is shown in equation (4.11).

$$F_g - F_b = V_p \left(\rho_s - \rho_g\right) g \tag{4.11}$$

The momentum balance is $F_{dr} = F_g - F_b$. And by writing this in a dimensionless form the correlation for terminal settling of a single particle system will be

$$\frac{3}{4} C_D(\mathrm{Re})\,\mathrm{Re}^2 = Ar \tag{4.12}$$

For a multiparticle system this correlation will be

$$\frac{3}{4} C'_D(\mathrm{Re}_s, \alpha_g)\,\mathrm{Re}_s^2 = Ar \tag{4.13}$$

Since the Archimedes number is assumed equal for a single and a multiparticle system, equation (4.12) and (4.13) can be coupled by the Archimedes number. And by rearranging the correlation between the drag factors will be like equation (4.14).

$$C'_D = C_D(\mathrm{Re})\frac{\mathrm{Re}^2}{\mathrm{Re}_s^2} = C_D(\mathrm{Re})\frac{\mathrm{Re}^{\,2}}{\mathrm{Re}_s} \tag{4.14}$$

It is introduced a new size which is the ratio between the terminal settling velocity of a particle in a multiparticle system and a isolated particle. This is the v_r, this is defined as (4.15).

$$v_r = \frac{v_{sys}}{v_{sphere}} \tag{4.15}$$

This expression can also relate the Reynolds numbers like equation (4.16).

$$\mathrm{Re} = \frac{\mathrm{Re}_s}{v_r} \tag{4.16}$$

By substituting equation (4.16) into equation (4.14) the relation between C_D and C'_D will be like equation (4.17).

$$C'_D(\mathrm{Re}_s, \alpha_g) = C_D\left(\frac{\mathrm{Re}_s}{v_r}\right)\frac{1}{v_r^2} \tag{4.17}$$

By using the C'_D instead of the C_D in the single particle drag model in equation (4.6) the drag model for the multiparticle system will be like equation (4.1). Then the drag factor C_D in the Syamlal O'Brien model is the single

particle drag factor given by Dalla Valle [22] modified for the multiparticle Reynolds number shown in equation (4.18).

$$C_D = \left[0.63 + \frac{4.8}{\sqrt{\frac{\mathrm{Re}}{v_r}}}\right]^2 \tag{4.18}$$

The velocity ratio v_r can be found experimentally from the Richardson and Zaki [23], but in the Syamlal O'Brien model the v_r is taken from the analytical formula by Garside and Al Dibouni [24]. This model is a curve fitted version of the Richardson and Zaki equations. The analytical formula is shown in equation (4.19).

$$\frac{v_r - A}{B - vr} = \frac{0.06\,\mathrm{Re}}{v_r} \tag{4.19}$$

If this formula (4.19) is solved for v_r the expression will be like equation (4.20).

$$v_r = \frac{1}{2}\left[A - 0.06\,\mathrm{Re} + \sqrt{(0.06\,\mathrm{Re})^2 + 0.12\,\mathrm{Re}\,(2B - A) + A^2}\right] \tag{4.20}$$

In this equation (4.20) A and B is defined as in (4.21).

$$\begin{aligned} A = &\quad \alpha_g^{4.14} \\ B = &\quad \begin{cases} 0.8\alpha_g^{1.28} & \alpha_g \leq 0.85 \\ \alpha_g^{2.65} & \alpha_g > 0.85 \end{cases} \end{aligned} \tag{4.21}$$

4.2 Gidaspow drag model

The drag model by Gidaspow is made out of two drag models, one for the dense regime and one for the dilute. This models are the Ergun equation and the Wen and Yu drag model. The Ergun equation is a model for pressure drop though a packed bed, and is assumed to be valid for fluidized condition by [4]. This model is valid for gas volume fractions $\alpha_g \leq 0.8$ [14]. For $\alpha_g > 0.8$ the drag correlation by Wen and Yu is used.

4.2.1 Derivation of the Ergun equation

To derive the Ergun equation [25] it is assumed a laminar flow through a tube. In this regime the viscose forces is strong. This flow can be described with the Poiseuille Law which is found in literature to be like equation (4.22).

$$Q = \frac{\pi r^4 \Delta p}{8\mu_g l} \tag{4.22}$$

In equation (4.22) Q is the volumetric flow rate, an l is the length of the tubes. This way of writing the Poiseuille Law is for calculating pressure drop or volumetric flow rate in pipes or wanes. This formula is favoured to have it on a form that can be used a general area rather than the specific area of the cross-sectional area of a tube. The volumetric flow rate Q is substituted with $A_{tube}u_{int}$ where the area is the area of the tube and the velocity is the interracial

velocity. By doing this substitutions and rewriting, the equation will be as in equation (4.23).

$$-\frac{\Delta p}{l} = \frac{u_{int} 32 \mu_g}{D^2} \tag{4.23}$$

Here is D the tube diameter. The interracial velocity v_{int} is a velocity which has to be rewritten because this is the velocity inside the tubes and when the porous media is concerned the tubes will not a real tube, but a channel through the porous media. The length of this tube is not the same as the length of the porous media. Then a new size is introduced , the tortuosity which is $\chi = \frac{l_{\text{real}}}{l}$ where the l_{real} is the total length of the tube and l is just the length of the porous media. Using this to describe the the interracial velocity by the superficial velocity and the tortuosity the expression for the pressure drop will be like equation (4.24).

$$\frac{\Delta p}{l} = \frac{32 \mu_g u \chi}{\alpha_g D^2} \tag{4.24}$$

Now u is the superficial velocity.

By assuming that the area of one side of the porous media can be written as $V_{tubes} + V_{solid}$ it can be expressed the tubes volume fraction and since this tubes is the channels in the porous media that is filled with a fluid the fluid volume fraction will be like in equation (4.25).

$$\alpha_g = \frac{V_{tubes}}{V_{tubes} + V_{solids}} \tag{4.25}$$

By solving equation (4.25) for V_{tubes} the expression will be like equation (4.26).

$$V_{tubes} = \frac{\alpha_g V_{solids}}{(1 - \alpha_g)} \tag{4.26}$$

The left hand side of equation (4.26) has to be divided by the surface area of tubes and the right hand side on the surface area of a sphere. Here the tube volume is the volume of n cylinders and the tube area is the area of n cylinders. The solids volume is the volume of n spheres and the area is the surface area of n spheres. The shape factor ϕ is also introduced to compensate for non spherical solids. The shape factor is defined as equation (4.27).

$$\phi = \frac{6\,(\text{Volume of the particle})}{d_p\,(\text{surface area of the particles})} \tag{4.27}$$

By doing this modifications to equation (4.26) the expression will be lie equation (4.28).

$$\frac{n \pi D^2 l_{pores}}{4 n \pi D l_{pores}} = \frac{\pi d_s^3 \phi \alpha_g}{6 \pi d_s^2 (1 - \alpha_g)} \tag{4.28}$$

This equation (4.28) can be simplified and solved by D and becomes like equation (4.29).

$$D = \frac{2 d_s \phi \alpha_g}{3 (1 - \alpha_g)} \tag{4.29}$$

By inserting the expression (4.29) for the tube diameter into equation (4.24) the expression for the pressure drop in a given direction say x will be like

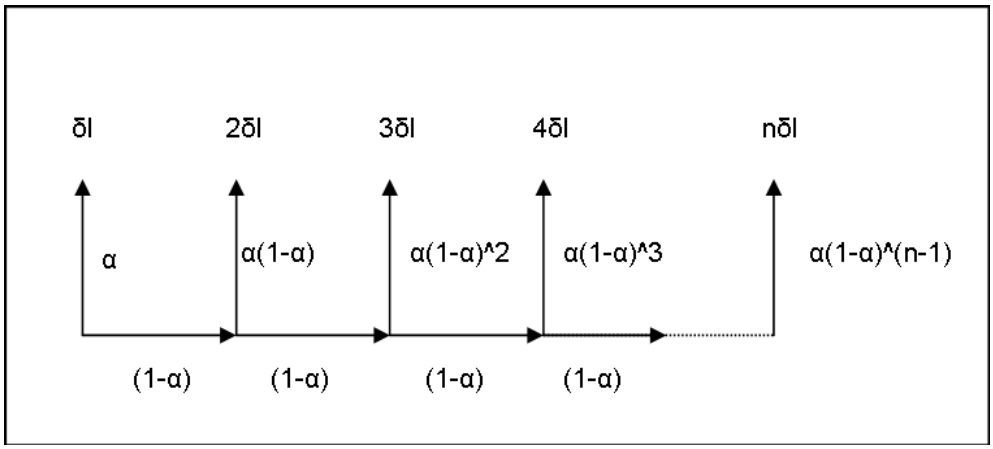

Figure 4.1: Probability tree for the constant in the Kozeny-Carman equation

equation (4.30).

$$-\frac{\partial p}{\partial x} = 72\frac{\mu_g u_x \left(1-\alpha_g\right)^2}{\left(d_s\phi\right)^2 \alpha_g^3}\chi \tag{4.30}$$

This equation (4.30) is the Kozeny-Carman equation and is used in the Ergun equation to describe the viscous, low Reynolds regime. The classical way to write the Ergun equation is to have the constant 72 equals 150. To obtain this the tortuosity equals a empirical constant $\frac{25}{12}$.

Another way to find this constant is to do a probabilistic analyses on the tortuosity. Concering a system without particles, the flow will go straight through. And when the solids occupy all the space the flow will not go through. This will be a asymptotic solution for both maximum and minimum solid fraction. Considering a length δl that the fluid can move. The probability that it is no solid particles in the length δl is α_g. The probability of particles occupying the space is $(1-\alpha_g)$. Considering a flow that will go twice the length, the probability for this will be $\alpha_g\left(1-\alpha_g\right)$. In Figure 4.1 the probability tree for the probabilities that the fluid will flow from one to n lengths, δl, in the flow direction.

By summarizing the probabilities that the probability that the flow will take one to n lengths, the expression will be $\sum_{n=1}^{\infty} n\delta l\alpha_g\left(1-\alpha_g\right)$. This will be the actual length the flow will move. The tortuosity is the actual length the flow move divided by the length of the porous media in the direction the flow moves the expression for the tortuosity will be like equation (4.31).

$$\chi = \frac{\sum_{n=1}^{\infty} n\delta l\alpha_g\left(1-\alpha_g\right)}{\delta l} = \frac{1}{\alpha_g} \tag{4.31}$$

The Ergun is valid for fluid volume fractions in the interval $\langle 0.4, 0.6\rangle$ [21]. The values of the tortuosity at the boundaries of the valid interval will be $\chi\left(\alpha_g = 0.4\right) = \frac{1}{0.4}$ and $\chi\left(\alpha_g = 0.6\right) = \frac{1}{0.6}$. By taking the mean value of this the

expression for the mean tortuosity will be like expression (4.32).

$$\overline{\chi} = \frac{\left(\frac{1}{0.4} + \frac{1}{0.6}\right)}{2} = \frac{25}{12} \tag{4.32}$$

The expression for the high Reynolds number flow in the Ergun equation is derived in the same manner but here it is considered turbulent flow. Here makes the kinetics of the flow a more dominant role than the viscous forces in the fluid [26]. In this flow regime the pressure drop is due to kinetic energy loss. This therm will have the form (4.33).

$$\frac{\partial p}{\partial x} = \frac{1}{D}\frac{\rho_g u_{int}^2}{2} \tag{4.33}$$

By multiplying equation (4.33) with a factor, it has the same form as the Darcy friction factor. For the laminar region the expression for the Darcy friction factor will be a simple expression of the Reynolds number, but in the turbulent region this will be a more complex expression. By using (4.33) multiplied with a factor and deriving in the same manner as the Kozeny-Carmann equation (4.30) the expression for the kinetic pressure loss will be (4.34).

$$\frac{\partial p}{\partial x} = \frac{f\chi^2 3}{4}\frac{\rho_g u^2 \left(1-\alpha_g\right)}{d_s \phi \alpha_g^3} \tag{4.34}$$

The first part of equation (4.34) $\left(\frac{f\chi^2 3}{4}\right)$ is hard to evaluate theoretically, and is therefor a empirical constant equal 1.75 in the Ergun equation. By substituting this into equation (4.34) the equation will be the Burke-Plummer equation [27] which the Ergun equation is based on.

By adding the Kozeny-Carman equation (4.30) and the Burke-Plummer equation (4.34) and using the empirical parameters the combination will be like equation (4.35).

$$-\frac{\partial p}{\partial x} = 150\frac{\mu_g u \left(1-\alpha_g\right)^2}{\left(d_s\phi\right)^2 \alpha_g^3} + 1.75\frac{\rho_g u^2 \left(1-\alpha_g\right)}{d_s \phi \alpha_g^3} \tag{4.35}$$

The correlation between the drag and the pressure drop in the Ergun equation is shown in equation (4.36), and is taken from the reference [4].

$$-\alpha_g \frac{\partial p}{\partial x} - K_{sg}\left(|\overrightarrow{u_g} - \overrightarrow{u_s}|\right) = 0 \tag{4.36}$$

By substituting equation (4.35) into equation (4.36) and rearranging and substituting for the interracial velocity in equation (4.36) the expression for the pressure loss will be like equation (4.37).

$$K_{sg} = 150\frac{\mu_g \left(1-\alpha_g\right)^2}{\alpha_g \left(d_s\phi\right)^2} + 1.75\frac{\rho_g \left(|\overrightarrow{u_g} - \overrightarrow{u_s}|\right)\left(1-\alpha_g\right)}{d_s\phi} \tag{4.37}$$

This equation (4.37) is the Ergun equation used in the drag model by Gidaspow.

4.2.2 Derivation of the Wen and Yu model

The Wen and Yu model is for the dilute regime and is based on the work by Richardson and Zaki in the reference [21]. This model is derived in the same manner as the drag model by Syamlal O'Brien derived in chapter 4.1 by finding the drag on several particles acting alone then modify this to a system of particles. The model for several single particles is shown in equation (4.38).

$$K_{sp} = \frac{3\rho_g \alpha_g \left(1-\alpha_g\right)}{4d_p} C_D \left|\overrightarrow{u_s} - \overrightarrow{u_g}\right| \tag{4.38}$$

The drag factor C_D is the drag factor for a single sphere and has to be substituted with the multiparticle drag factor C'_D by equation (4.39).

$$C_D = f\left(\alpha_g\right) C'_D \tag{4.39}$$

The factor $f\left(\alpha_g\right)$ is taken from Richardson and Zaki and is a experimental factor which is valid when the internal forces is negligible which means that the viscous forces dominate the flow behavior. The factor is $f\left(\alpha_g\right) = \alpha_g^{4.65}$. This factor has to be modified to fit Fluent 6.3 definition of particle Reynolds number. The factor from Richardson and Zaki is based on the relative settling velocity of a single sphere to a sphere acting in a system. This velocities and the Reynolds number is based on the superficial velocities. In Fluent 6.3 this is based on the interracial velocity. The single sphere drag factor is also corrected. The single sphere drag model is the Schiller and Neumann model [28] and his is derived for another definition of the Reynolds number. The result of this modifications is implemented in equation (4.38) will be the multiparticle drag function by Wen and Yu shown in equation (4.40).

$$K_{sg} = \frac{3\rho_g \alpha_g \left(1-\alpha_g\right)}{4d_p} C_D \left|\overrightarrow{u_s} - \overrightarrow{u_g}\right| \alpha_g^{-2.65} \tag{4.40}$$

where C_D is the single particle drag factor by Schiller and Naumann shown in equation (4.41).

$$C_D = \frac{24}{\alpha_g \operatorname{Re}_s} \left[1 + 0.15 \left(\alpha_g \operatorname{Re}_s\right)^{0.687}\right] \tag{4.41}$$

In the original model by Schiller and Neumann another definition for Reynolds number higher than 1000 is made. In a fluidized bed this Reynolds number is not possible to achieve since the velocity used is the relative velocity. The combination of large particles and high pressure operation is a case when it can be encountered. In Fluent 6.3 this high Reynolds drag is not used.

4.3 Richardson and Zaki

Lots of drag models is based on the experimental studies by Richardson and Zaki [23]. They related the terminal settling velocity of a single sphere in a infinite media, to the terminal settling velocity of particles in a system. It has also been investigated the effect of shape of the particles.

Richardson and Zaki did lots of experiments on relative settling velocities of both spheric and non-spheric particles particles. In the model whose been implemented in this work is only the spheric particles.

The relative settling velocity can be defined as equation (4.42).

$$\frac{v_s\,(\text{particle in system})}{v_s\,(\text{sphere})} = v_{r,s} = v_r \tag{4.42}$$

In equation (4.42) $v_{r,s}$ is the relative settling velocity. In a fluidized bed the settling velocity is not a interesting value to investigate. In a fluidized bed this model is used for modeling a fluid flowing trough particles rather than particles falling through the fluid. The relative velocity of the particles to the fluid surrounding it will be the same which means that $v_{r,s} = v_r$. The model for the relative velocity correlation v_r is shown in equation (4.43).

$$v_r = \alpha_g^n \tag{4.43}$$

This correlation in equation (4.43) is for the interracial velocity and it is favored to work with the superficial velocity, so the correlation will be like equation (4.44).

$$v_r = \alpha_g^{n-1} \tag{4.44}$$

The n parameter is the Richardson and Zaki parameter. It is a function of the particle Reynolds number Re_s divided by the relative velocity correlation v_r called the modified Reynolds number Re_m and is a piecewise function shown in equation (4.45).

$$n = \begin{cases} 4.65 & \mathrm{Re}_m < 0.2 \\ 4.4\,\mathrm{Re}_m^{-0.03} & 0.2 > \mathrm{Re}_m < 1 \\ 4.4\,\mathrm{Re}_m^{-0.1} & 1 > \mathrm{Re}_m < 500 \\ 2.4 & \mathrm{Re}_m > 500 \end{cases} \tag{4.45}$$

It is not a straight forward way to find the correlation because it is given implicit. It have to be used a iterative algorithm. The steps are:

1. Calculate particle Reynolds number with equation (4.46).

$$\mathrm{Re}_s = \frac{d_p \rho_g \, |\overrightarrow{u_g} - \overrightarrow{u_s}|}{\mu_g} \tag{4.46}$$

2. Guess a value for the relative velocity correlation v_r e.g. 1.

3. Calculate the modified Reynolds number with equation (4.47).

$$\mathrm{Re}_m = \frac{\mathrm{Re}_s}{v_r} \tag{4.47}$$

4. Use the calculated Re_m to calculate the parameter n in equation (4.45).

5. Calculate right hand side of equation (4.44).

6. Check if the guessed v_r and the calculated v_r in step 5. match. If not use the new v_r in step 3 and calculate it one more time until convergence. The error accepted in this work is 10^{-5}.

It is several ways to use the relative velocity correlation v_r for calculating the drag [21] but in this work the derivation of the Syamlal and O'Brien drag model is used. The derivation is further described in chapter 4.1. The difference in the Richardson and Zaki model is that the analytical model for the relative velocity correlation v_r in equation (4.20) from Garside and Al-Dibouni is not used [21]. This will result in a iterative drag model who is like equation (4.48).

$$K_{sg} = \frac{3\alpha_g \alpha_s \rho_g}{4 d_s v_r^2} C_D \left| \overrightarrow{u_s} - \overrightarrow{u_g} \right| \tag{4.48}$$

In this equation (4.48) v_r is calculated by the Richardson and Zaki parameters from equation (4.45) and C_D is calculated with the model from Dalla Valle [22] which is shown in equation (4.18).

The C-code for the user defined function for the Richardson and Zaki drag function is found in appendix B.

4.4 RUC-drag model

The RUC or Representative Unit Cell model is based on pressure drop through porous media. It was originally proposed by Du Plessis and Masliyah in 1988 [29] for isotropic spong-like media. The RUC for granular media was made by Du Plessis and Masliyah in 1991 [**??**]. The latest version of the RUC who is used in this work is made by Du Plessis in 1994 [21]. The derivation of this model is shown in the reference [32]. The model is also better explained in the reference [32]. In this work the RUC is just briefly explained.

This model is a modification of the Ergun equation. The Ergun equation is derived in the chapter 4.2.1. The RUC model uses the same models as the Ergun equations uses. The Kozeny-Carman equation describe the viscous regime and the Burke-Plummer equation describe the turbulent regime. The difference is that the RUC model uses analytically derived constants rather than the semi-empirical coefficients 150 and 1.75 used in the Ergun equation.

From the viscous regime part of the Ergun equation the particle phase is assumed to be uniformly distributed smooth spherical particles. The fluid phase is assumed to flow though parallel tubes which have a length adjusted by the tortuosity [32]. In the RUC model the particle phase is assumed to be cubes. The configuration of the cubes have two possibilities, either regular or staggered. By using an average geometry between this positions an expression for the pattern the flow will follow is made. The result of this averaging is used with other relations and a model for the semi-empirical constant 150 in the Kozeny-Carman is made and called A. This A can be expressed as equation (4.49) and is shown as a function of the fluid volume fraction in Figure 4.2.

$$A = \frac{26.8\alpha_g^3}{\left(1-\alpha_g\right)^{2/3}\left(1-\left(1-\alpha_g\right)^{1/3}\right)\left(1-\left(1-\alpha_g\right)^{2/3}\right)^2} \tag{4.49}$$

This model might look empirical cause of the number 26.8 but this number is due to the geometrical averaging and is shown how to find in the reference [32].

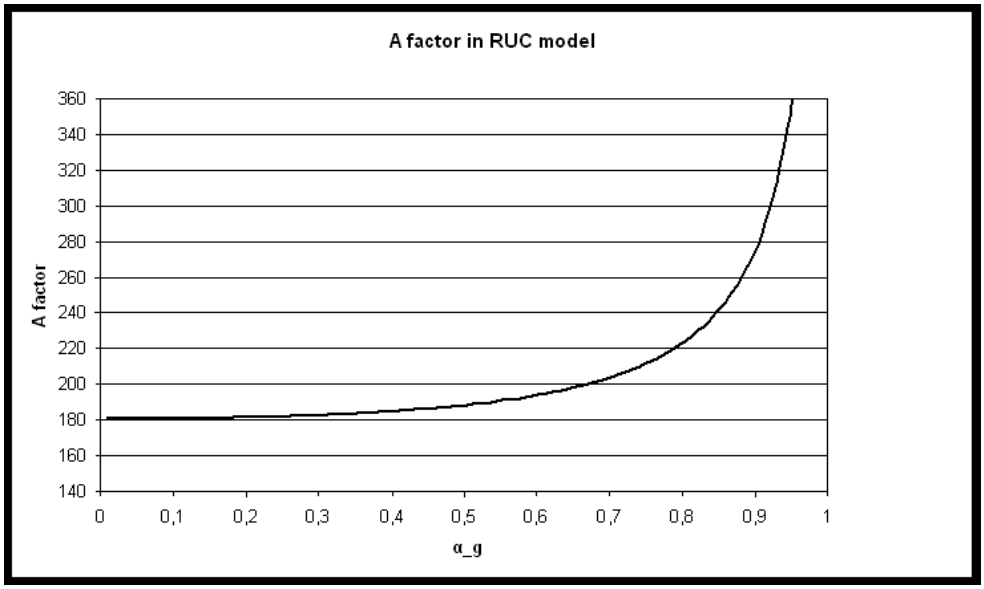

Figure 4.2: The constant A in the RUC model

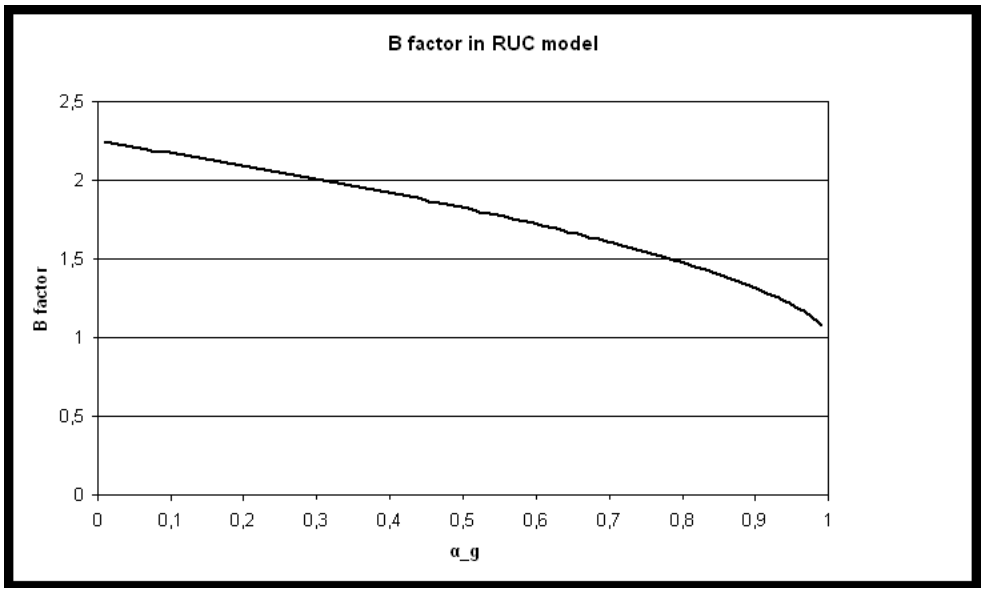

Figure 4.3: The constant B in the RUC model

The other coefficient in the RUC model is for the Burke-Plummer equation. In the Ergun equation this coefficient is 1.75, which is called B in the RUC model. This coefficient can be written as equation (4.50) and is shown as a function of fluid volume fraction in Figure 4.3.

$$B = \frac{\alpha_g^2}{\left(1-(1-\alpha_g)^{2/3}\right)^2} \tag{4.50}$$

The RUC drag model will with this models for A and B become like equation (4.51).

$$K_{sg} = \frac{26.8\alpha_g^3}{\left(1-(1-\alpha_g)^{1/3}\right)\left(1-(1-\alpha_g)^{2/3}\right)^2}\frac{\mu_g\left(1-\alpha_g\right)^{4/3}}{\alpha_g {d_s}^2} + \frac{\alpha_g^2}{\left(1-(1-\alpha_g)^{2/3}\right)^2}\frac{\rho_g\left(|\overrightarrow{u_g}-\overrightarrow{u_s}|\right)\left(1-\alpha_g\right)}{d_s} \tag{4.51}$$

The RUC drag model is implemented in Fluent 6.3 by the author with a user defined function and the C-code is shown in appendix A.

4.5 Hill Koch Ladd Drag correlation

The Hill Koch Ladd drag correlation is based on data from Lattice-Boltzmann simulations [33]. The Lattice-Boltzmann model, LBM, is a alternative for solving the Naiver-Stokes equations. This model use statistical fluid dynamic to describe the flow behavior. In the LBM the computational domain is build out of a lattice. This lattice might have different configurations. In the lattice it is lattice nodes where the "strings" making the lattice cross. Every node holds a set of variables, which is the particle distribution function f_i. This variables will give information to all the neighbouring nodes. The distance to the neighbouring nodes is $\overrightarrow{c_i}$ and the position of the lattice node is $\overrightarrow{r}$. The model for the LBM is like equation (4.52).

$$f_i\left(\overrightarrow{r}+\overrightarrow{c_i}, t+\Delta t\right) - f_i\left(\overrightarrow{r}, t\right) = \Omega_i \tag{4.52}$$

The Ω_i is the collision term and describe the interaction between the variables in the lattice compared to the neighboring nodes.[34]

The further theory and solving algorithms of the LBM has not been studied in this work.

The model by Hill Koch Ladd is build on this LBM and fitted for a model describing the interphase momentum exchange between the phases (drag) in a granular multiphase flow. The model for the drag by Hill Koch Ladd is very accurate for a limited range of void fractions and Reynolds numbers. Benyahia, Syamlal and O'Brien has extended this work to cover the full range of void fractions and Reynolds number expected in a fluidized bed and is valid for one solid phase. The drag model is defined by equation (4.53).

$$K_{sg} = 18\mu_g \alpha_g^2 \alpha_s \frac{F}{d_p^2} \tag{4.53}$$

The factor F in equation (4.53) is a dimensionless drag factor. This can also be expressed in the more familiar way for Fluent 6.3 users. This is expressed in equation (4.54).

$$K_{sg} = \frac{3}{4}\frac{C_D \alpha_s \alpha_g \rho_g \left|\overrightarrow{u_g} - \overrightarrow{u_s}\right|}{d_p} \tag{4.54}$$

Where C_D can be expressed as (4.55).

$$C_D = 12\frac{\alpha_g^2}{\mathrm{Re}_s}F \tag{4.55}$$

In the Hill Koch Ladd drag model the characteristic length of the flow is the radius of the particles rather than the diameter that is the most used in the granular models. This will result in that the particle Reynolds number Re_s will be defined as equation (4.56).

$$\mathrm{Re}_s = \frac{\rho_g \alpha_g d_p \left|\overrightarrow{u_g} - \overrightarrow{u_s}\right|}{2\mu_g} \tag{4.56}$$

In the work by Benyahia, Syamlal and O'Brien [33] is the derivation and blending of the modified Hill Koch Ladd drag model used in this study. The result of the modification is presented here.

The model starts with defining some factors w, F_0, F_1, F_2 and F_3. This is shown in equation (4.57, 4.58, 4.59, 4.60, 4.61).

$$w = e^{(-10(0.4-\alpha_s)/\alpha_s)} \tag{4.57}$$

$$F_0 = \begin{cases} (1-w)\left[\frac{1+3\sqrt{\alpha_s/2}+(135/64)\alpha_s\ln(\alpha_s)+17.14\alpha_s}{1+0.681\alpha_s-8.48\alpha_s^2+8.16\alpha_s^3}\right]+w\left[10\frac{\alpha_s}{(1-\alpha_s)^3}\right] & 0.01<\alpha_s<0.4 \\ 10\frac{\alpha_s}{(1-\alpha_s)^3} & \alpha_s \geq 0.4 \end{cases} \tag{4.58}$$

$$F_1 = \begin{cases} \frac{\sqrt{\frac{2}{\alpha_s}}}{40} & 0.01<\alpha_s\leq 0.1 \\ 0.11+0.00051e^{(11.6a_s)} & \alpha_g > 0.1 \end{cases} \tag{4.59}$$

$$F_2 = \begin{cases} (1-w)\left[\frac{1+3\sqrt{\alpha_s/2}+(135/64)\alpha_s\ln(\alpha_s)+17.89\alpha_s}{1+0.681\alpha_s-11.03\alpha_s^2+15.41\alpha_s^3}\right]+w\left[10\frac{\alpha_s}{(1-\alpha_s)^3}\right] & \alpha_s<0.4 \\ 10\frac{\alpha_s}{(1-\alpha_s)^3} & \alpha_s \geq 0.4 \end{cases} \tag{4.60}$$

$$F_3 = \begin{cases} 0.9351\alpha_s+0.03667 & \alpha_s<0.0953 \\ 0.0673+0.212\alpha_s+0.0232/\left(1-\alpha_s\right)^5 & \alpha_s\geq 0.0953 \end{cases} \tag{4.61}$$

This factors are used in the drag model to model the dimensionless drag factor F which is a piecewise function of Reynolds number and solids volume fraction. The piecewise functions for F is shown in equation (4.62).

$$\begin{array}{ll} F = 1+3/8\,\mathrm{Re}_s & \alpha_s \leq 0.01 \text{ and } \mathrm{Re}_s \leq \dfrac{(F_2-1)}{(3/8-F_3)} \\ F = F_0+F_1\,\mathrm{Re}_s^2 & \alpha_s > 0.01 \text{ and } \mathrm{Re}_s \leq \dfrac{F_3+\sqrt{F_3^2-4F_1\left(F_0-F_2\right)}}{2F_1} \\ F = F_2+F_3\,\mathrm{Re}_s & \text{Otherwise} \end{array} \tag{4.62}$$

This drag model is implemented into Fluent 6.3 by the author. The C-code for the user defined function is shown in appendix C

Chapter 5

Turbulence modeling

Simulations including the different turbulence models in Fluent 6.3 are performed. They are:

- Laminar (no modeling of turbulence)
- k-ε (standard, RNG, realizable)
  - dispersed
  - mixture
  - per phase
- RSM (Reynold stress model)
  - dispersed
  - mixture

In a bubbling fluidized bed the packing regime will be from dense to dilute. The dispersed k-ε and RSM are only valid for the dilute regime in a bubbling fluidized bed and will by this reason not be appropriate for usage in fluidized bed simulations [1]. The mixture model uses mixture velocity and density to calculate the turbulence. This is appropriate when the density ratio between the phases close to one [1]. This is not be the case in a bubbling fluidized bed used in this work where the gas density is approximately 1 kg/m^3 and the particle density is approximately 2500 kg/m^3. The k-ε -per phase will calculate the turbulence behavior of all of the phases and then combine them [1]. This means that two additional transport equations for each secondary phase has to be calculated [1]. This means that the calculation will be very complex.

k-ε with per phase calculation and the laminar or no turbulence model is the only suitable models in this case. In the reference [36] it is claimed that it is no need for a turbulence model in a bubbling fluidized bed.

In this study Fluent 6.3 is used to evaluate the bubble behavior with or without a turbulence model. A two dimensional fluidized bed grid with a central jet in the bottom of the bed is used to investigate the bubble behavior. By investigating the bubble behavior the turbulence model was chosen. To choose the correct version of the k-ε model (std, RNG or realizable) is an own field and has not been investigated by theory only simulations.

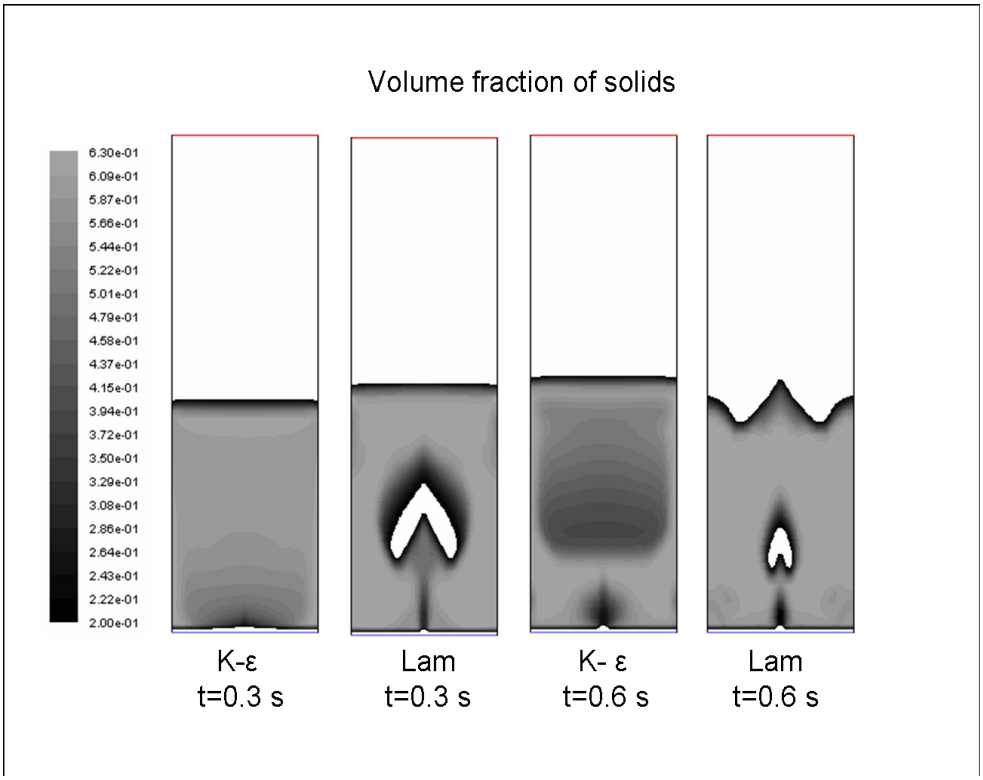

Figure 5.1: Comparison of bubble behaviour with and without turbulence model

The results show that the turbulence model dispersed the momentum in the jet and the bubble did not get the appropriate size and form.

For other work at Telemark University College by the reference [35] the LES (large eddy simulations) and a SGS (subgrid scale)model is used to calculate the turbulence [35]. The LES models all the large eddies and not average them and the SGS models the small eddies. Fluent 6.3 has no option for LES when simulating with multiphase flow. [1]

The Figure 5.1 show the bubble behavior with and without a turbulence model.

5.1 Computational setup for the 2D case with jet

The aim of this study is to evaluate the bubble behavior of one bubble rather than the bubbling frequency or any other parameter. Different models and discretization schemes are used in the simulation. The grid resolution was increased, but the trend of the result did not vary to much. The different simulation setups is not shown here cause it was made to investigate the usage of turbulence models or not. The result shows a similar trend that the k-ε was not appropriate for the case and it was assumed that it was not appropriate to use

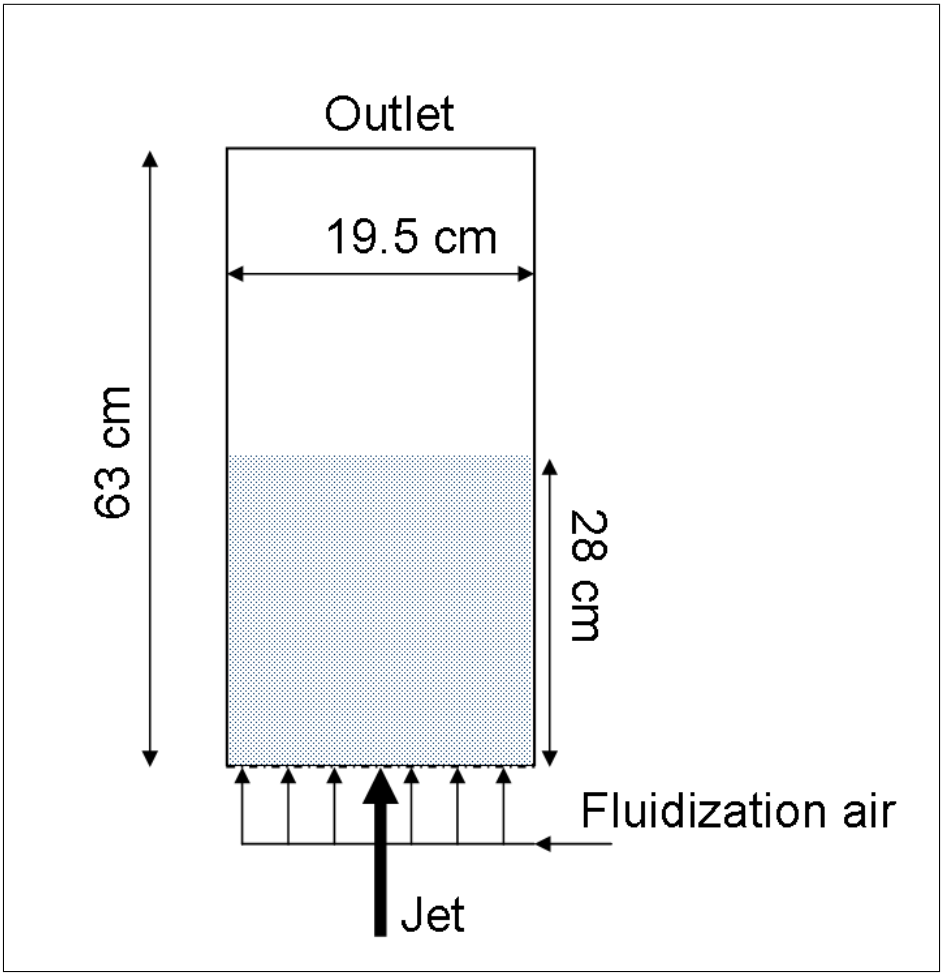

Figure 5.2: The 2D fluidized bed with jet used to investigate the bubble behaviour

a turbulence model in the 3D simulations also.

The grid used had a resolution of 1cm x 0.5 cm. It was tried with a mesh with the resolution of 0.5 cm x 0.25 cm. This is shown in Figure 5.2. In Table 5.1 the data of the bubbling fluidized bed with jet is shown.

All this data in Table 5.1 is taken from the work by the reference [35] but some are modified.

5.2 Conclusion

The conclusion from this work is that it is best to not use any turbulence models in the bubbling fluidized bed simulations in Fluent 6.3 because it is not any ideal model implement in Fluent yet. The bubble form of the laminar simulations conserves more of the momentum in the jet.

Jet velocity	4.9 m/s	Air density	1.225 kg/m^3
Fluidization velocity	0.29 m/s	Height of bed	63 cm
Particle diameter	491 μm	Width of bed	19.5 cm
Solids density	2485 kg/m^3	Initial height of particles	28 cm
Initial solid fraction	0.6	Maximum solid fraction	0.63
Air viscosity	1.7894x10^{-5} kg/m·s	Operating pressure	101325 Pa

Table 5.1: Properties used in the 2D case to investigate the usage of turbulence models

In the case with the k-ε turbulence model, the momentum get dispersed by the turbulence model, which is a known phenomena with the k-ε model. And the conclusion in the reference [36] has the same opinion as this work has.

Part II

Simulations of bubbling fluidized bed

Chapter 6

3D simulations of fluidized bed

6.1 Computational setup for 3D simulations of fluidized bed

In the 3D case the domain is made after the work and experimental rig by the reference [35]. It is a 3D fluidized bed with the height of 2 meters. The cross-sectional area is 25 cm x 25 cm. This fluidized bed has a uniform gas distribution in the bottom. Experimental data in this fluidized bed is made by the reference [35]. This results are used to compare the results from the simulations.

The first case investigated was to use the default settings in Fluent 6.3 and just vary the drag model. The discretization scheme used in this part is the first order upwind scheme.

In the 3D case a hexagonal grid with cubic cells with the side length of 1 cm was used. A figure of the fluidized bed is shown in Figure 6.1.

The simulation setup which was used in the 3D case is shown in Table 6.1.

The default settings for Fluent 6.3 for the granular phase properties is shown in Table 6.2.

Height of bed	200 cm	Initial bed height	75 m
Width of bed	25 cm	Initial solids fraction	0.6
Length of bed	25 cm	Maximum solids fraction	0.64356
Particle diameter	154 μm	Fluidization air velocity	0.133 m/s
Particle density	2485 kg/m^3	Air viscosity	1.7894x10^{-5} kg/m·s
Air density	1.225 kg/m^3	Operating pressure	101325 Pa

Table 6.1: Simulation setup used in the 3D case

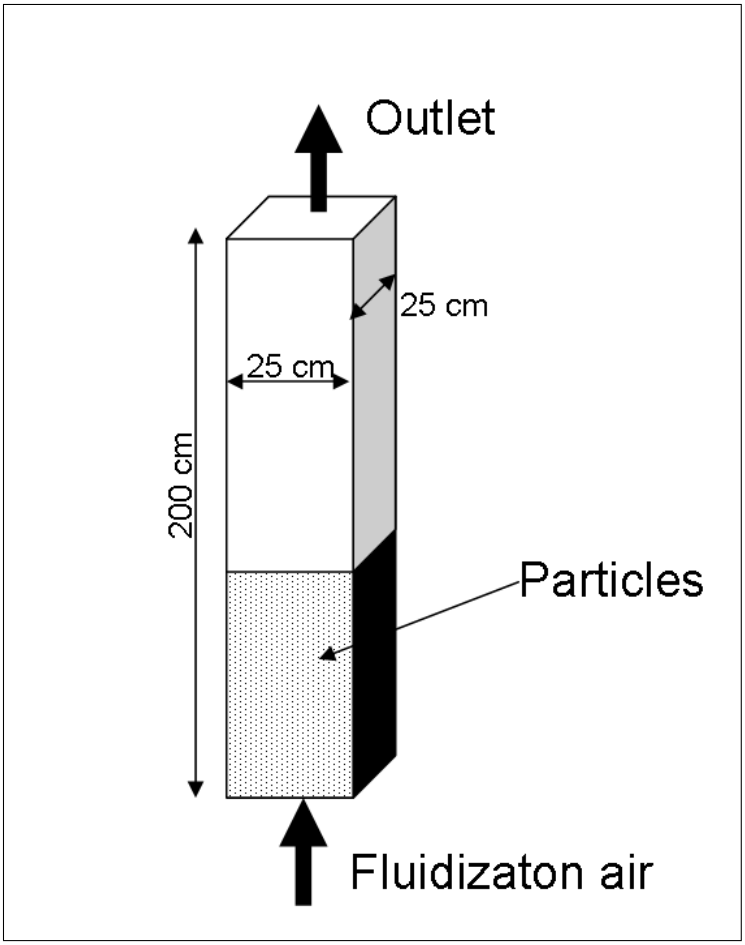

Figure 6.1: The dimensions 3D fluidized bed

Granular viscosity	constant = 1x10^{-5}
Granular bulk viscosity	constant = 0
Frictional viscosity	none
Angle of internal friction	na
Frictional pressure	na
Granular temperature	algebraic
Friction packing limit	na
Solids pressure	Lun et al
Radial distribution	Lun et al

Table 6.2: Defoult settings for the granular properties in Fluent 6.3

6.2 Review of the simulations of a 3D fluidized bed

The main interest of this case was to investigate the default settings in Fluent 6.3 and see the result of this in bubble frequency. A bubble is defined as volume fraction of particles lower than 0.35. The results show that the defaults settings in Fluent 6.3 do not match the bubble frequencies predicted in the experimental work by the reference [35]. The conclusion from this work is to further investigate which models to use to get the best results and find out which parameters to change to get a better solution.

This work with the build in drag models and the default settings for the granular properties has resulted in a paper made by Britt Halvorsen and the author. This paper is found in appendix D.

Chapter 7

2D simulations of fluidized bed

7.1 Computational setup for 2D simulations of fluidized bed

In this part of the study the data is based on experimental results in a 3D bubbling fluidized bed with uniform air distribution in the bottom by the reference [35].

Some of the difficulties involving 3D simulations is that the computational resources are limited which result in large computational time. The computational resources available in this work has resulted in computational time of one and a half week per case. The study is limited to 2D and assumed to have the same characteristics as the 3D case.

This study is divided into five part which is described individually. All the cases will have the same computational setup as the 3D simulations in chapter 6 except the case with more than one particle phase. The width of the bed equal zero because this case is a 2D case. The models used in the different cases are varying. A base case for the study is made.

The particle diameter is taken from the work by the reference [35] and is the mean particle diameter for the particles use in the experimental rig. This diameter is 154 μm.

A partial differential equation to calculate the granular temperature is used. This will enable more models to describe the granular flow. This means that it is solved a own transport equation for the granular temperature and convection and diffusion will not be neglected.

The granular viscosity is chosen to be described by the model of Syamlal and O'Brien. This model is chosen because it is based on the kinetic theory of granular flow (KTGF) by Lun et al.

The granular bulk viscosity is chosen to be described by Lun et al. This model describes the deformation of the bulk flow.

The frictional viscosity is set to use Schaeffers equation. The Schaeffer equation uses the second invariant of the deviatoric stress tensor and mathematically describe the phenomena happening in the frictional regime.

The angle of internal friction is set to 28.5^0 which is used some references [12].

The frictional pressure is set to based-KTGF. This means that the pressure used to calculate the frictional viscosity is the solids pressure. By choosing the correct model for solids pressure and radial distribution a asymptotic behavior of the frictional pressure, which is the case when the solids fraction converges the maximum packing limit.

The frictional limit is set to 0.5 cause this is used some references [12].

The granular conductivity is set to Syamlal and O'Brien. This model is derived from the KTGF by Lun et al.

The solids pressure is set to Lun et al cause it describe the increase in solids pressure both by the collisions between particles and the kinetic energy in the particles.

The radial distribution is set to Lun et al. This model is chosen cause it is taken from the KTGF and it will have a asymptotic solution when the solids fraction increase.

The maximum packing of solids in the bed is 0.64356 and is taken from the reference [35].

The discretization scheme in the base case is first order upwind.

The simulation time is set to 30 seconds with time steps of 0.001 seconds.

The drag model used in the base case is the Syamlal O'Brien.

7.2 Case 1: Discretization scheme

Different discretization scheme was studied in this case of the simulation of a bubbling fluidized bed and simulated was performed with a first and second order upwind scheme. The case with the second order upwind scheme had the same computational setup as the base case except the discretization scheme. The theory behind the discretization scheme can be found in the reference [35]. The main parameter investigated was the bubble frequency. Investigation of the mean solid fraction where performed.

The results from the simulation is shown in Figure 7.1 where the simulations with first and second order upwind scheme are compared. The experimental data is included for comparison.

The Figure 7.1 show the results closest to the experimental data is the simulations with the second order upwind scheme.

Simulations with other higher order discretization schemes like the QUICK-scheme are performed, but this results were quite similar to the results of the second order upwind scheme. This higher order discretization schemes is not further investigated and it is assumed that the behavior of the bubbling fluidized bed is best described by the second order upwind scheme.

The mean solid fraction in both cases show quite similar results and is not further investigated.

7.3 Case 2: Usage of frictional regime

Simulations with and without the usage of the frictional regime where performed. The frictional viscosity describing the frictional behavior of the flow

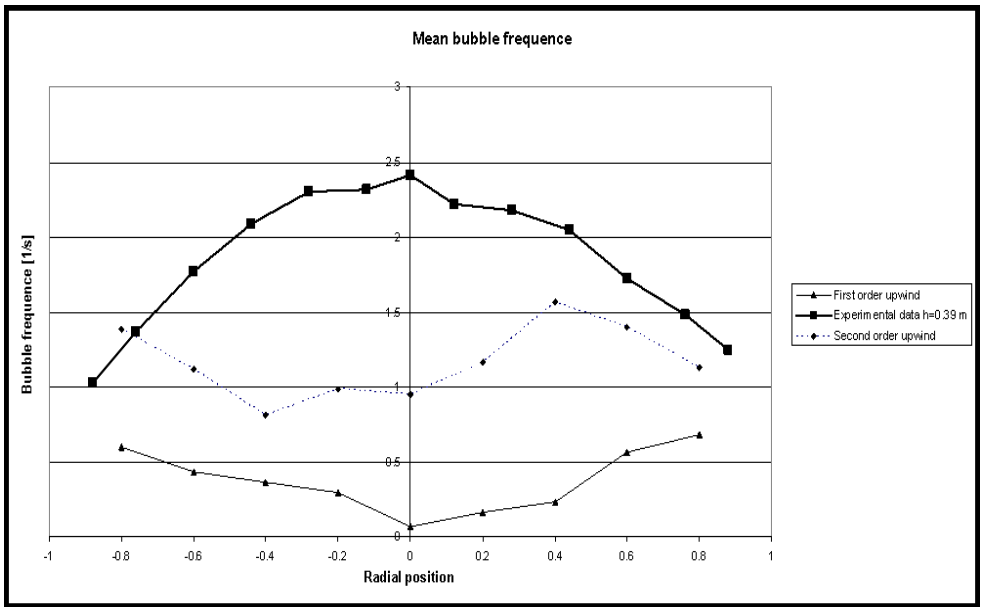

Figure 7.1: Comparison of first order and second order upwind scheme

will make the granular flow act plastic. This theories are often based on soil mechanics and have a empirical nature. The models used in this case for the frictional regime is mostly based on mathematics and kinetic theory of granular flow.

In this case it is also used the result from the first case that the flow is best described by the second order upwind scheme. Both cases, with and without frictional regime, is done with second order upwind scheme.

The results from this simulations is shown in Figure 7.2.

Figure 7.2 shows quite similar results with and without a frictional regime. The calculations for the frictional regime is quite complicated and takes a lot of computational effort. Since the simulations gave so close results in bubbling frequency , the frictional regime is not used further in this work .

7.4 Case 3: Drag model

The main interest in this study was to investigate the interfacial momentum exchange between phases. This can be described by a drag model. In Fluent 6.3 two build in drag models for dense fluidized beds is included, which is the case in this study. Three other drag models are included by user defined functions in Fluent 6.3. The drag models used in the simulation is

- Gidaspow
- Syamlal O'Brien
- RUC

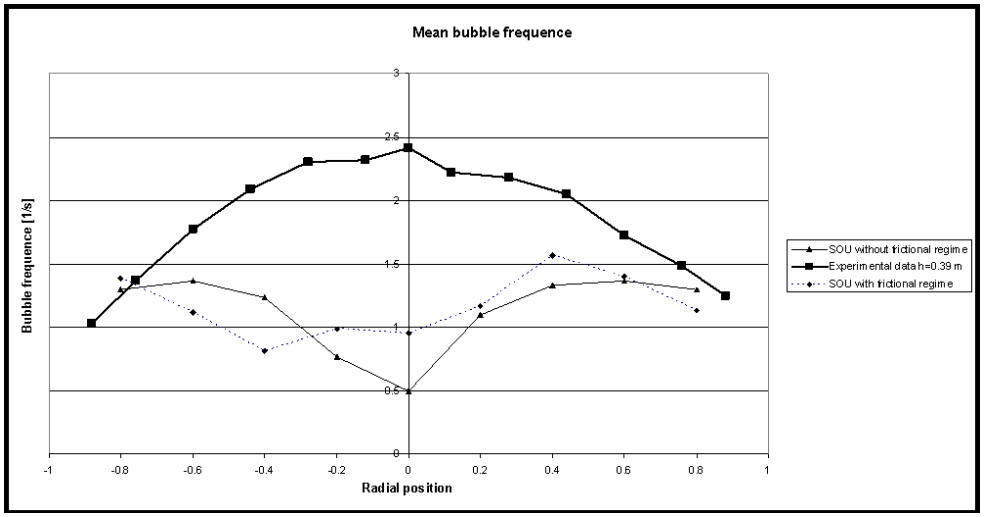

Figure 7.2: Comparison between frictional regime and no frictional regime

Diameter	154 μm
Fluidization air velocity	0.133 m/s
Air density	1.225 kg/m^3
Air viscosity	1.7894x10^{-5} kg/m·s
Slip velocity	0.133/α_g m/s

Table 7.1: Parametrers used as the input parameters in the drag models

- A modified Syamlal and O'Brien model with iterative Richardson and Zaki parameters called the Richardson and Zaki.
- A Hill Koch Ladd drag correlation

All this drag models are described in detail in chapter 4.

The different drag models will predict a drag. Figure 7.3 show the predicted drag as a function of solids fraction.

The parameters used to make this Figure 7.3, is taken from Table 7.1.

As shown in Table 7.1 the slip velocity is the fluidization air velocity divided by the volume fraction of air. What is meant with slip velocity is the velocity of the fluid compared to the solids when the particles are fixed in position. Figure 7.3 show that the drag correlation by Hill Koch Ladd and the RUC predict the highest drag and Richardson and Zaki predict the lowest. The characteristics of the drag models are a little bit different and it seems like they will predict very different drag at high solid fractions. The Hill Koch Ladd is very different from the other models at low solids fraction.

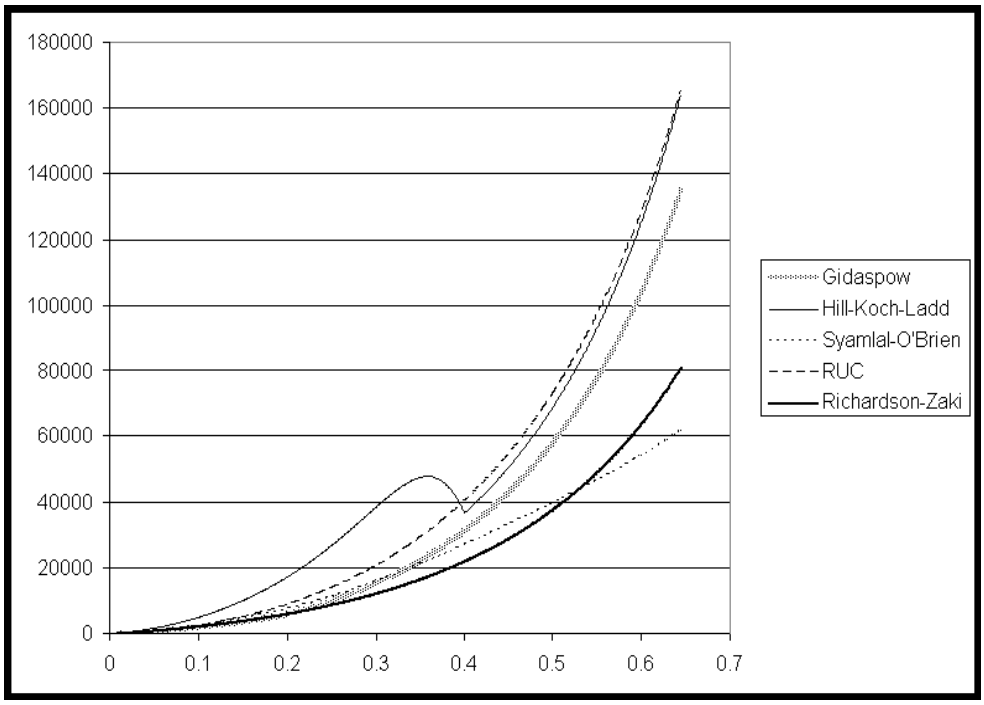

Figure 7.3: The different drag predicted by the different drag models

The simulations are made with the assumptions from the other cases that second order upwind discretization scheme and no frictional regime gives the best results.

Figure 7.3 show the drag as a function of solids fraction and Figure 7.4 is the mean solids fraction at the height of 39 cm from simulations with Fluent 6.3.

Figure 7.4 show similar results to the one dimensional analyses of the drag models 7.3.

The bubble frequency of the different drag models is shown in Figure 7.5.

The bubbling frequencies predicted with the drag models differ significantly. The graph of the results from the simulations show that the RUC and the Hill Koch Ladd model predict the highest bubbling frequency. The results is actually very interesting because these models are rather new and are mathematically developed. The RUC is build on a geometric formulation of the solid phase and the Hill Koch Ladd is made of Lattice-Boltzmann simulations with a origin in statistical fluid mechanics.

7.5 Case 4: Multiple particle phases

In the experimental work on the fluidized bed by the reference [35] it is used particles with the mean size of 154 μm, but the particles have a distribution shown in Figure 7.6. It means the particles have lots of different sizes. This will affect the simulations because of a size distribution.

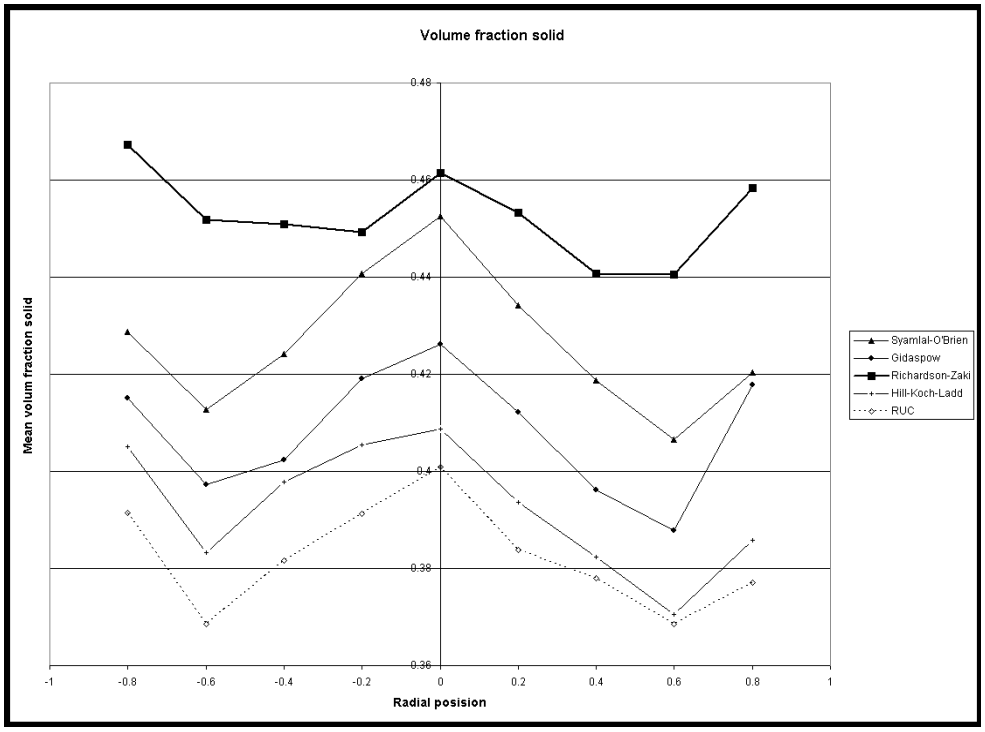

Figure 7.4: The mean solids volume fraction at different radial posisions taken from the simulation results

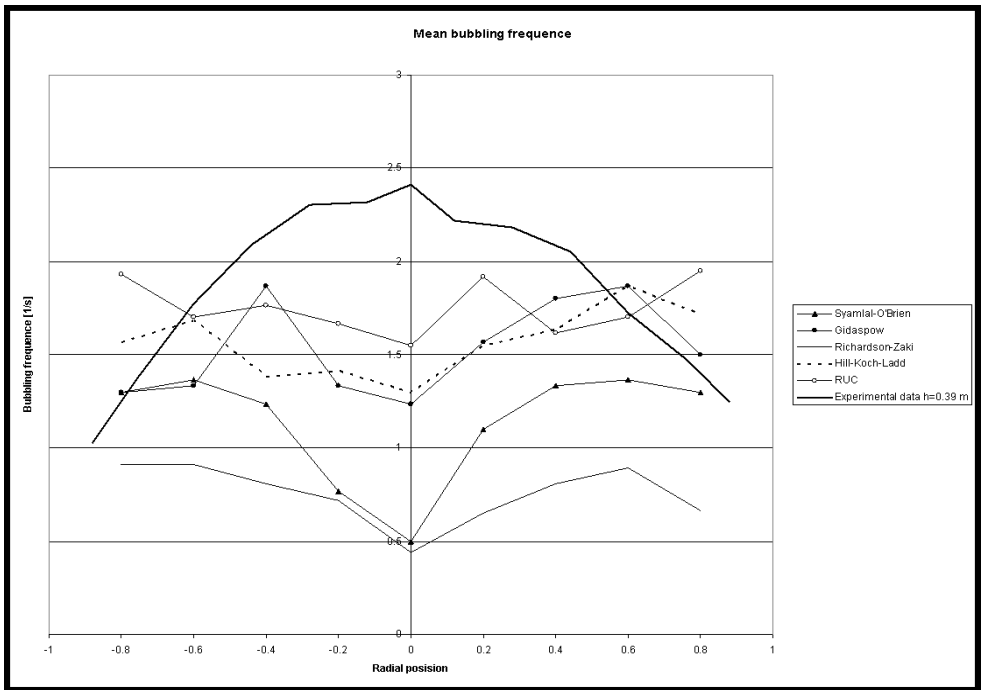

Figure 7.5: Bubble frequency at different radial posisions for the different drag models

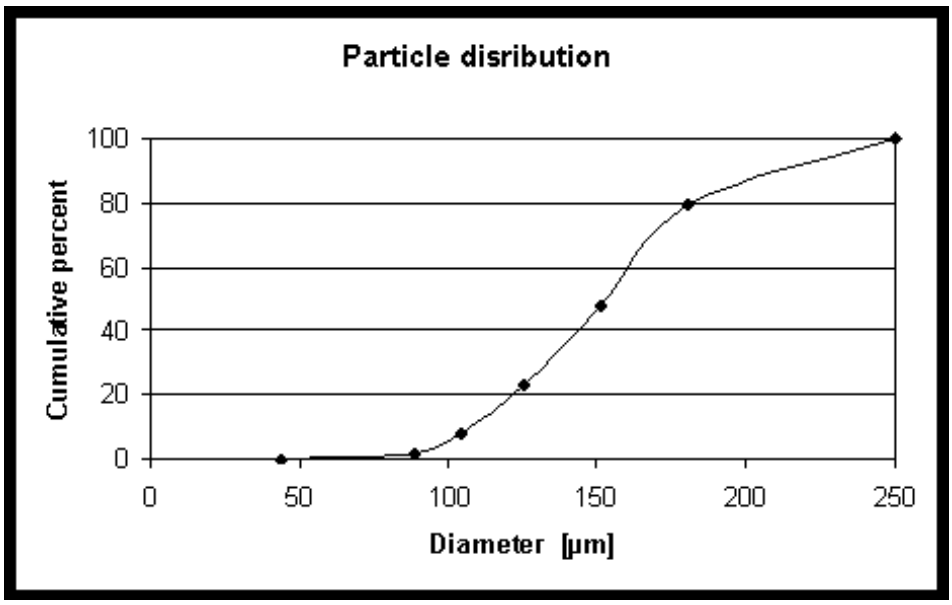

Figure 7.6: The size distribution for the particles used in the experiments [35]

Particle diameter [μm]	percentage
100	24%
150	36%
190	40%

Table 7.2: Simplified particle distribution

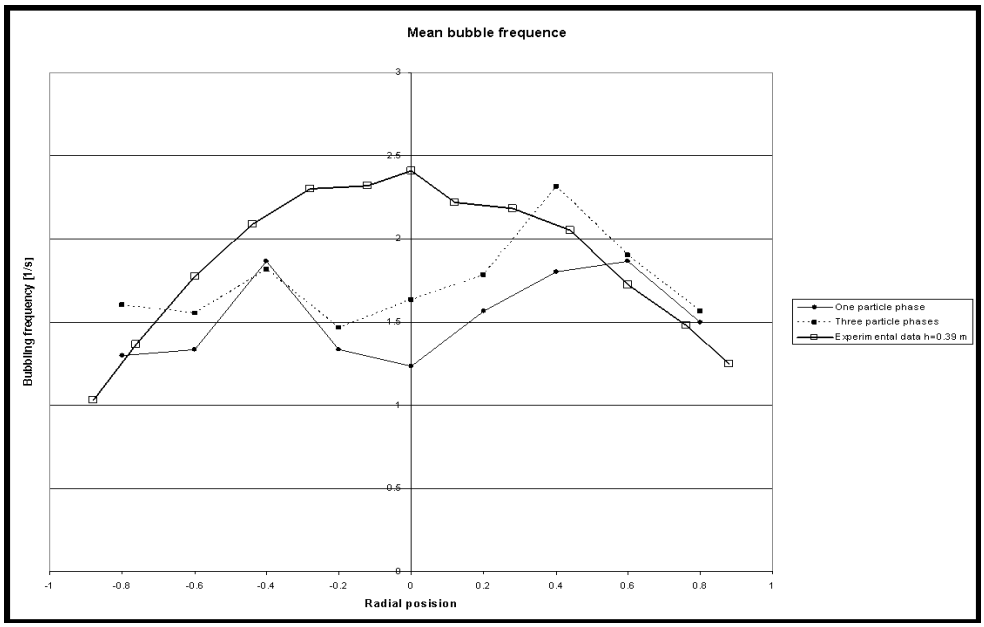

Figure 7.7: Comparison for simulation results with one and three particle phases

To account for the particle size distribution in the simulations three particle phases are included. By trial and error a combination of particle sizes and percentage of each phase that will give a mean diameter of 154 μm is found. This combination is shown in Table 7.2.

For the simulations in this case it was used the result from earlier cases which means second order upwind scheme and no frictional regime. The drag model used in this part of the study is the Gidaspow drag model. This model gave a acceptable bubbling frequency and it is already build in Fluent 6.3. The Hill Koch Ladd is just valid for one particle phase so it is not used.

The simulations with three particle phases needs a drag model to describe the particle-particle drag between the solid phases. The option for particle-particle drag in Fluent 6.3 is the symmetric Syamlal O'Brien. This model is not investigated any further just used in this case. For a description read the [1].

The results showed the bubbling frequency increased by including more particle phases. Figure 7.7 show the bubble frequency predicted by Gidaspow drag model with one particle phase and the case with three particle phases. The experimental results is also included in comparison.

The Figure 7.7 show that the bubbling frequency will go up with more particle phases. This introduction of more particle phases will give a more real

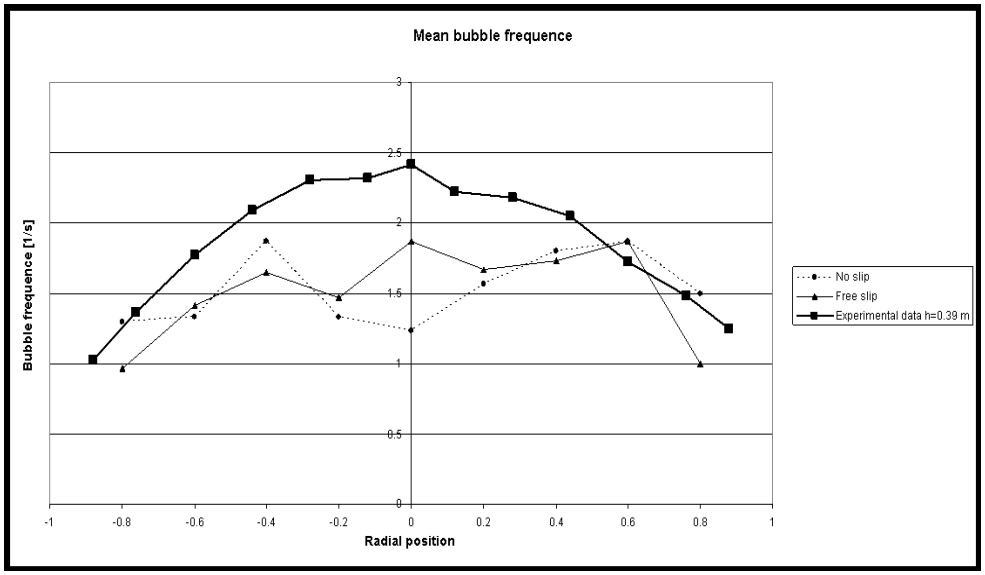

Figure 7.8: Comparison of no slip and free slip condisions at the walls

result because it will be closer to the real case. The simulations show that the mean bubbling frequency will go up by approximately 0.2 bubbles per second with the Gidaspow drag model using three particle phases rather than just one.

7.6 Case 5: Introducing other wall functions

In this case it is used the same computational setup as the setup in case 3 and the Gidaspow drag model. The difference in this case is that the wall functions in Fluent 6.3 is changed from no slip to free slip for the solid phase. The results from case 3 gave the highest bubbling frequencies on both sides of the vertical center line in the bed, and not in the center as the experimental data.

A theory by the author why the bubble frequency distribution profile is not similar to the experimental data. Because of the grid resolution a thick boundary layer of particles at the boundaries by the walls with make the particles stand still. This will cause the particles to move easier in the center of the bed compared to at the walls. This is not a theory verified by other references, but with simulations. The theory of boundary conditions is not further investigated.

The results of introducing a free slip condition at the walls where the Gidaspow with no slip and free slip is compared to the experimental data is shown in Figure 7.8.

The Figure 7.8 show that the simulations with free slip and no slip have approximately the same bubbling frequency, but the simulations with free slip have the some shape as the experimental data.

7.7 Review of the simulations of a 2D fluidized bed

The results from the simulations of a 2D fluidized bed show that the Hill Koch Ladd and the RUC predicted the bubbling frequency closest to the experimental data. Since the Hill Koch Ladd drag model is only valid for one particle phase is the most reasonable model for further investigations is the RUC model.

The simulations give the best results with more particle phases. In the case where the number of particle phases is investigated, the Gidaspow drag model is used. For further investigation the RUC should be tried implemented for multiple particle phases.

For the boundary conditions the simulations show that free slip is giving a better result. The case with free slip is most likely not physically correct but it is most likely better than no slip.

A modified case of the result is made from the single particle phase Gidaspow drag model result with free slip boundary conditions at the walls of the fluidized bed. The difference in the mean bubbling frequency by changing from Gidaspow to RUC is approximately 0.22 bubbles per second. The difference in the case with Gidaspow drag model with one particle phase to the case with three particle phases is approximately 0.2 bubbles per second. By doing this modifications to the free slip simulations with the Gidaspow drag model the modified results from the simulations will be like Figure 7.9 where it is compared with the experimental results.

This Figure 7.9 is not showing a actual simulation, but it is a modified version of on case including contributions from other effect. The simulation time in the cases used in all of this work is set to 30 seconds. By increasing the time it is expected to get a smoother curve and the bubbling frequency will match the experimental results.

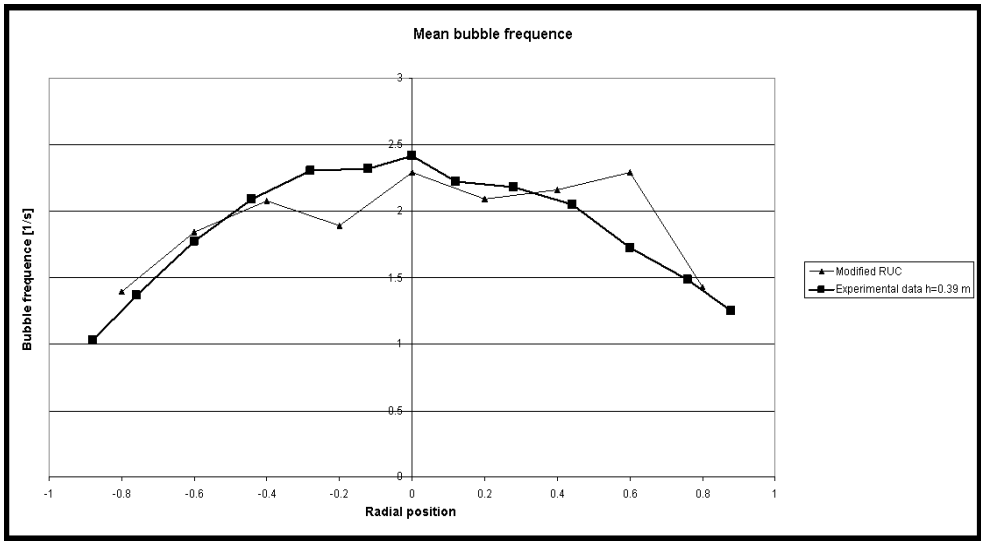

Figure 7.9: The modified results form the simulations made by combining three results

Chapter 8

Conclusion

This work has resulted in simulations of both 2D and 3D. The main focus in this work is simulations of the 3D experimental rig. Simulations in 3D was performed, but this simulations was to computational expensive to do for all the cases done. With this conclusion it was chosen to assume that 2D simulations could represent what was happening in the 3D fluidized bed.

The 2D simulation of the fluidized bed with jet, was used to investigate the usage of turbulence model. The conclusion of the simulations was to use no turbulence model (laminar) gave the best results.

In the study of the experimental rig in 3D simulations was performed in 2D. The work was divided into five cases to investigate different aspects of the case. The cases was:

- Choose of discretization scheme
- Usage of frictional regime
- Comparisons of drag models
- Multiple particle phases
- no slip or free slip conditions at the boundaries

In the first case a second order upwind scheme was chosen. This gave the results closes to the experimental data.

The frictional regime was not used. The conclusion was made cause the results of the case with and without frictional regime was very similar, and the case with frictional regime is more computational expensive.

In the case where the drag models was compared the RUC and the Hill Koch Ladd showed the best results of the bubble frequency. The Richardson and Zaki model was the one who showed the lowest bubbling frequency. The Gidaspow drag model showed the highest bubbling frequencies for the build in drag models for dense fluidized beds in Fluent 6.3.

In the case where multiple particle phases was investigated there was used the Gidaspow drag model. The reason for this is was because it is build-in in Fluent 6.3 and the RUC and Hill Koch Ladd is not. The Hill Koch Ladd is just made for one particle phase. The RUC model is possible to use for multiple phases but needs to be implemented with a user defined functions in Fluent

6.3. This was not done for more than one particle phase. The results from the Gidaspow model with more particle phases showed a better result than the case with just one particle phase.

The effect of boundary conditions in the walls in the fluidized bed was investigated. It was used free and no slip conditions at the walls, and the case with free slip gave a more similar bubble frequency distribution compared to the experimental data than the no slip case.

The theory behind the models used to describe the properties was investigated and assumed by the author that the kinetic theory of granular flow by Lun et al gave the best representation of the granular behavior of the flow and particles.

The conclusion of this work is that Fluent 6.3 is a good tool to investigate this type of problem with bubbling fluidized beds. The drag model with the largest potential to give the best result is the RUC model with free slip conditions at the walls, second order upwind discretization scheme, multiple particle phases and no turbulence model.

The work with the 3D simulations with the default properties models has resulted in a paper for the conference HEFAT2008 conference in South Africa. This paper is found in appendix D.

The study of drag models in this work will result in a paper for the SIMS2008 conference in Oslo 2008. The focus of this paper will be the comparison of drag models. The abstract for this paper is in appendix E.

The suggested simulation setup from this work will be further investigated in later work. The suggestions is found in the chapter 9.

Chapter 9

Future works

With the experience from this works it is made some suggestions for future works related to this case. This suggestions are:

- Wall functions

It is tried out to change from the default no slip to free slip condition at the boundaries at the walls. This change has been shown to give better result. The suggested action in future works is to investigate other wall functions and see the result of this. It is also suggested to look at the grid resolution at the walls.

- Multiple particle phases

It is tried out to use multiple particle phases and the results got closer to the experimental results. It is suggested to use multiple particle phases in all the cases investigated to see the effect on the drag models with the best results in the single phase simulations. The results from the simulations show that the RUC and the Hill Koch Ladd drag models gives the results closest to the experimental data. This drag models are implemented in Fluent 6.3 with user defined functions which is written in C code. This functions are not made for more than one particle phase and is suggested to be modified for more particle phases. The Hill Koch Ladd drag model is not valid for more than one particle phase, but the RUC is valid and suggested to be implemented.

- Comparing 2D and 3D simulations

It is assumed that the 2D presentation of the bubbling fluidized bed gives similar results to the 3D presentation. This assumption is not investigated if it is good or not. This can be done by doing the suggested cases from the conclusion from this work in 3D.

- Averaging time

It is assumed that the simulations time of 30 seconds give a good result. The result show that this might be to little because the results is not symmetric around the central axes. The problem is assumed to be corrected as the simulation time is increased.

Chapter 10

References

1. Fluent 6.3 User guide, September 2006.
2. Lun C. K. K., Savage S. B., Je rey D. J. and Chepurniy N., "Kinetic Theories for Granular Flow: Inelastic Particles in Couette Flow and Slightly Inelastic Particles in a General Flow Field". J. Fluid Mech., vol 140, pp 223-256, 1984.
3. M. Syamlal, W. Rogers and O'Brien T. J., "MFIX Documentation: Volume 1, Theory Guide. National Technical Information Service, Spring eld, VA", 1993. DOE/METC-9411004, NTIS/DE9400087.
4. Gidaspow D., "Multiphase Flow and Fluidization-Continuum and Kinetic Theory Descriptions". Academic Press, San Diego , 1994.
5. Jenkins, J. T., and Savage S. B. , "A Theory for the Rapid Flow of Identical, Smooth, Nearly Elastic Spherical Particles", J. Fluid mech. vol 130, pp 187, 1983.
6. Ding J. and Gidaspow D. ,"A Bubbling Fluidization Model Using Kinetic Theory of Granular Flow". AIChE J., vol 36, no4, pp 523-538, 1990.
7. Huilin L., Yurong H., Wentie L., Ding J., Gidaspow D. and Bouillard J,. "Computer simulations of gas-solid flow in spouted beds using kinetic-frictional stress model of granular flow"., Chemical Engineering Science, vol 59, pp 865 – 878, 2004.
8. Hu W. and Wang Z. R., "Distortion stress, distortion strain and their physical concept"., J. Matherial Processing Technology, vol 121 pp 202-206, 2002.
9. Internet site: http://www.engin.umich.edu/class/bme456/ch2stress/bme456stress.htm, 02/04-2008.
10. Schaefer D. G. , "Instability in the Evolution Equations Describing Incompressible Granular Flow"., J. Diff. Eq., vol 66, pp 19-50, 1987.
11. Johnson P. C. and Jackson R. , "Frictional-Collisional Constitutive Relations for Granular Materials, with Application to Plane Shearing"., J. Fluid Mech., vol 176, pp 67-93, 1987.

12. Johnson P. C., Nott P. and Jackson R. "Frictional-collisional equations of motion for particulate Flows and their application to chutes"., Journal of Fluid Mechanics, vol 210, pp 501–535., 1990.

13. Ocone R., Sundaresan S. and Jackson R., "Gas-particle flow in a duct of arbitrary inclination with particle-particle interaction"., AIChE J., vol 39, pp 1261-1271, 1993.

14. Enwald H., Peirano E., Almstedt A. E., "Eulerian Two-Phase Flow Theory Applied to Fluidization"., Int. J. Multiphase Flow, vol 22, pp 21-66, 1996.

15. Chapman S. and Cowling T. G., "The Mathematical Theory of Non-Uniform Gases"., Cambridge University Press, Cambridge, England, 3rd edition, 1990.

16. Ogawa S. , Umemura A. and Oshima N. , "On the Equation of Fully Fluidized Granular Materials"., J. Appl. Math. Phys., vol 31, pp 483, 1980.

17. Lebowitz J. L., "Exact Solution of Generalized Percus-Yevick Equation for a Mixture of Hard Spheres"., The Phy. Rev., vol 133, no 4A, pp A895-A899, 1964.

18. Ma D. and Ahmadi G. "A Thermodynamical Formulation for Dispersed Multiphase Turbulent Flows". Int. J. Multiphase Flow, vol 16 no 2, pp 323-351, 1990.

19. Ibdir H. and Arastoopour H. "Modeling of multi-type particle flow using kinetic approach". AICHE Journal, May 2005.

20. Alder B. J., Wainwright T. E. "Studies in molecular dynamics. II. Behavior of small number of elastic spheres". J Chem Phys. vol 33 pp: 2363-2382, 1960.

21. Syamlal M., O'Brien T. J., "The Derivation of a Drag Coefficient Formula from Velocity-Voidage Correlations", April 1987.

22. Dalla Valle J. M. , "Micromeritics"., Pitman, London, 1948.

23. Richardson J. F. and Zaki W. N., "Sedimentation and Fluidization: Part I," Trans. Inst., Chem. Eng., vol 32, pp 35-53, 1954.

24. Garside J. and Al-Dibouni M. R. , "Velocity-Voidage Relationships for Fluidization and Sedimentation"., I & EC Process Des. Dev., vol 16, pp 206-214, 1977.

25. Ergun S. , "Fluid Flow through Packed Columns". Chem. Eng. Prog., vol 48, no 2, pp 89-94, 1952.

26. Niven R. K., "Physical insight into the Ergun and Wen & Yu equation for fluid flow in packed and fluidized beds"., Chemical Eng. Science, vol 57, pp 527-534, 2002.

27. Burke S. P., Plummer W. B., "Gas Flow through Packed Columns", vol 20, no 11, pp 1196, 1928.

28. Schiller L. and Naumann. Z. Ver. Deutsch. Ing., vol 77, pp 318, 1935.

29. Du Plessis J. P. and Masliyah J. H., "Mathematical Modeling of Flow Through Consolidated Isotropic Porous Media"., Transport in Porous Media, vol 3, pp 145-161, 1988.

30. Du Plessis J. P. and Masliyah J. H., "Flow Through Isotropic Granular Porous Media"., Transport in Porous Media, vol 6, pp 207-221, 1991.

31. Du Plessis J. P., "Analytical Quantification of Coeficients i the Ergun Equation for Fluid Friction in a Packed Bed"., Transport in Porous Media, vol 16, pp 189-207, 1994.

32. Woudberg S., "Laminal flow through Isotropic Granular Porous Media"., Master thesis at the University of Stellenbosch, December 2006.

33. Benyahia S., Syamlal M. and O'Brien T.J., "Extension of Hill Koch Ladd drag correlation over all ranges of Reynolds number and solids volume fractions"., Powder Tec., vol 162, pp 166-174, 2006.

34. Lätt J., "Hydrodynamic Limit of Lattice Boltzmann Equations". Doctorial thesis at Université de Genève, 2007.

35. Halvorsen B., "An Experimental and Computational Study of Flow Behaviour in Bubbling Fluidized Beds". Doctorial thesis at NTNU, 2005.

36. Goldschmidt M, "Hydrodynamic Modeling of Fluidized Bed Spray Granulation"., Doctoreal thesis at Universiteit Twente, August 2001.

Appendix A

Code for RUC drag model in 2D

```
/*************************************************************************
The drag model propsed by Du Plessis 1994 and implemented in Fluent 6.3 by
Lundberg and Halvorsen 2008 for one particle phases and 2 dimensions
*************************************************************************/

#include "udf.h"
#include "sg_mphase.h"

#define diam2 0.000154


/*define paricle diamtre for phase*/

DEFINE_EXCHANGE_PROPERTY(drag_ruc, cell, mix_thread, s_col, f_col)
{
 Thread *thread_g, *thread_s;
 real x_vel_g, x_vel_s, y_vel_g, y_vel_s, abs_v, slip_x, slip_y,
      rho_g, mu_g, afac, bfac, void_g, void_s, vfac, k_g_s, he, het;


 /* find the threads for the gas (primary) and solids (secondary phases).
These phases appear in columns 2 and 1 in the Interphase panel respectively*/

 thread_g = THREAD_SUB_THREAD(mix_thread, s_col);/*gas phase*/
 thread_s = THREAD_SUB_THREAD(mix_thread, f_col);/* solid phase*/


 /* find phase velocities and properties*/

 x_vel_g = C_U(cell, thread_g);
 y_vel_g = C_V(cell, thread_g);
```

```
 x_vel_s = C_U(cell, thread_s);
 y_vel_s = C_V(cell, thread_s);

 slip_x = x_vel_g - x_vel_s;
 slip_y = y_vel_g - y_vel_s;

 rho_g = C_R(cell, thread_g);

 mu_g = C_MU_L(cell, thread_g);


 /*compute slip*/

 abs_v = sqrt(slip_x*slip_x + slip_y*slip_y);


/*get the void fractions*/

 void_g = C_VOF(cell, thread_g);/* gas vol frac*/
 void_s = C_VOF(cell, thread_s);/* s_phase vol frac*/


/* make a helping size*/

he = pow(1.-void_g, (2./3.));
het = pow(1.-void_g, (1./3.));


/*compute drag and return drag coeff, k_g_s*/

 if(void_g>0.99)
  afac = 785.0;
 else
  afac = (26.8*void_g*void_g*void_g)/(he*(1.-het)*(1.-he)*(1.-he));

 if(void_g>0.01)
  bfac = (void_g*void_g)/((1.-he)*(1.-he));
 else
  bfac = 2.25;


 k_g_s = afac*void_s*(1-void_g)*mu_g/(void_g*pow(diam2, 2.))+bfac*rho_g*void_s*abs_v/diam2

 return k_g_s;

}
```

Appendix B

Code for Richardson and Zaki drag model in 2D

```
/*****************************************************************************
This udf is for customizing the drag model of Syamlal and Tom O'Brien with
the iterative method by Richardson and Zaki
for the velocity ratio Vr.

It works for 2d and one particle phase.

This is made by

Joachim Lundberg

*****************************************************************************/

#include "udf.h"
#include "sg_mphase.h"
#include "stdio.h"

#define diam2 0.000154


/*define paricle diamtre for phase*/

DEFINE_EXCHANGE_PROPERTY(rz_drag, cell, mix_thread, s_col, f_col)
{
 Thread *thread_g, *thread_s;
 real x_vel_g, x_vel_s, y_vel_g, y_vel_s, abs_v, slip_x, slip_y,
      rho_g, mu_g, afac, bfac, void_g, void_s, vfac, k_g_s, reyp,
      corr, reys, vrn, nn, taup, rho_s, fdrgs;

 int counter;
```

```
 /* find the threads for the gas (primary) and solids (secondary phases).
These phases appear in columns 2 and 1 in the Interphase panel respectively*/

 thread_g = THREAD_SUB_THREAD(mix_thread, s_col);/*gas phase*/
 thread_s = THREAD_SUB_THREAD(mix_thread, f_col);/* solid phase*/


 /* find phase velocities and properties*/

 x_vel_g = C_U(cell, thread_g);
 y_vel_g = C_V(cell, thread_g);

 x_vel_s = C_U(cell, thread_s);
 y_vel_s = C_V(cell, thread_s);

 slip_x = x_vel_g - x_vel_s;
 slip_y = y_vel_g - y_vel_s;

 rho_g = C_R(cell, thread_g);
 rho_s = C_R(cell, thread_s);

 mu_g = C_MU_L(cell, thread_g);


 /*compute slip*/

 abs_v = sqrt(slip_x*slip_x + slip_y*slip_y);


/*get the void fraction*/

 void_g = C_VOF(cell, thread_g);/* gas vol frac*/


/*calculating reynolds number*/

reyp = diam2*rho_g*abs_v/mu_g;


/*calculating Richardson Zaki parametrers for vr*/

vfac = 1.;
corr=1.;
counter=1;

while(corr>0.0001)
{
 reys = reyp/(vfac+SMALL);

  if (reys <= 0.2)
```

```
    nn = 4.65;

  else if (reys > 0.2 && reys <= 1.0 )
    nn = 4.4*pow(reys,-0.03);

  else if (reys> 1.0 && reys <= 500.)
    nn = 4.4*pow(reys,-0.1);

  else
    nn = 2.4;

vrn = pow(void_g,nn-1.);

corr=sqrt((vfac-vrn)*(vfac-vrn));

vfac=vrn;

counter++;

}


 /* compute particle relaxation time */

 taup = rho_s*diam2*diam2/18./mu_g;


 /*compute drag and return drag coeff, k_g_s*/

fdrgs = void_g*(pow((0.63*sqrt(reyp)/vfac+4.8*sqrt(vfac)/vfac),2.))/24.0;


 k_g_s = (1.-void_g)*rho_s*fdrgs/taup;

return k_g_s;
}
```

Appendix C

Code for Hill Koch Ladd drag correlation in 2D

```
/************************************************************************
This udf is for usin the Hill Koch Ladd correlation. This correlation is
made out of Lattice-Boltzmann simulations.
Benyahia, Syamlal and O'Brien has modified this correlations and
implemented this in MFIX. Then Mr. Lundberg has implemented
this in Fluent for 2d and one particle phase.

This is made by:

Joachim Lundberg

************************************************************************/

#include "udf.h"
#include "sg_mphase.h"
#include "stdio.h"

#define diam2 0.000154


/*define paricle diamtre for granular phase*/

DEFINE_EXCHANGE_PROPERTY(drag_HKL, cell, mix_thread, s_col, f_col)
{
 Thread *thread_g, *thread_s;

 real x_vel_g, x_vel_s, y_vel_g, y_vel_s, abs_v, slip_x, slip_y,
      rho_g, mu_g, void_g, void_s, k_g_s, reyp, rho_s,
      wfac, f0, f1, f2, f3,fac;


 /* find the threads for the gas (primary) and solids (secondary phases).
```

```
These phases appear in columns 2 and 1 in the Interphase panel respectively*/

 thread_g = THREAD_SUB_THREAD(mix_thread, s_col);/*gas phase*/
 thread_s = THREAD_SUB_THREAD(mix_thread, f_col);/* solid phase*/


 /* find phase velocities and properties*/

 x_vel_g = C_U(cell, thread_g);
 y_vel_g = C_V(cell, thread_g);

 x_vel_s = C_U(cell, thread_s);
 y_vel_s = C_V(cell, thread_s);

 slip_x = x_vel_g - x_vel_s;
 slip_y = y_vel_g - y_vel_s;

 rho_g = C_R(cell, thread_g);
 rho_s = C_R(cell, thread_s);

 mu_g = C_MU_L(cell, thread_g);


 /*compute slip*/

 abs_v = sqrt(slip_x*slip_x + slip_y*slip_y);


/*get the void fractions*/

 void_g = C_VOF(cell, thread_g);/* gas vol frac*/
 void_s = C_VOF(cell, thread_s);/* s_phase vol frac*/


/*calculating reynolds number*/

reyp = diam2*rho_g*abs_v*void_s/(2.*mu_g);


/*compute some factor*/

wfac=exp(-10.*(0.4-void_s)/(void_s+SMALL));


/* computing drag factors fac0, fac1, fac2, fac3*/

if(void_s>0.01 && void_s<0.4)
  f0 = (1.-wfac)*((1.+3.*sqrt(void_s/2.)+(135./64.)*
  void_s*log(void_s)+17.14*void_s)/
  (1.+0.681*void_s-8.48*void_s*void_s+8.16*void_s*void_s*void_s))+
```

```
  wfac*(10.*void_s/(void_g*void_g*void_g));
else if(void_s>=0.4)
  f0 = (10.*void_s/(void_g*void_g*void_g));
else
  f0 =0;

if (void_s>0.01 && void_s<=0.1)
  f1 = sqrt(2./void_s)/40.;
else if (void_s>0.1)
  f1 =0.11+0.00051*exp(11.6*void_s);
else
  f1 = 0;

if (void_s<0.4)
  f2 = (1.-wfac)*((1.+3.*sqrt(void_s/2.)+(135./64.)*void_s*
  log(void_s+SMALL)+17.89*void_s)/
  (1.+0.681*void_s-11.03*void_s*void_s+15.41*void_s*void_s*void_s))+
  wfac*(10.*void_s/(void_g*void_g*void_g));
else
  f2 = (10.*void_s/(void_g*void_g*void_g));

if(void_s<0.0953)
  f3 = 0.9351*void_s+0.03667;
else
  f3 = 0.0673+0.212*void_s+0.0232/pow(void_g,5.);


/*finding the correct drag functions*/

if(void_s<=0.01 && reyp<=((f2-1.)/(3./8.-f3)))
  fac = 1.+3./8.*reyp;
else if (void_s>0.01 && reyp<=((f3+sqrt(f3*f3-4.*f1*(f0-f2)))/(2*f1)))
  fac = f0+f1*reyp*reyp;
else
  fac = f2+f3*reyp;


 k_g_s = 18.*mu_g*void_g*void_g*void_s*fac/(diam2*diam2);

return k_g_s;
}
```

Appendix D

Paper for the Conference HEFAT2008 in South Africa

HEFAT2008
6th International Conference on Heat Transfer, Fluid Mechanics and Thermodynamics
30 June to 2 July 2008
Pretoria, South Africa
Paper number:HB1

COMPUTATIONAL STUDY OF BUBBLING FLUIDIZED BED

Britt M. Halvorsen[a,b], Joachim Lundberg[a], Vidar Mathiesen[c]
a. Telemark University College, Norway
b. Telemark Technological R&D Centre (Tel-Tek), Norway
c. StatoilHydro, Norway
E-mail: britt.halvorsen@hit.no

ABSTRACT

This work presents a computational study of flow behaviour in a bubbling fluidized bed. The model is developed by using the commercial CFD code Fluent 6.3. The model is based on an Eulerian description of the gas and the particle phase. Different drag models are used and compared. The computational results are validated against experimental results.

The experimental data are based on measurements performed by Britt Halvorsen in 2004. The dimension of the lab-scale fluidized bed is 0.25x0.25x2.00 m. The simulations are performed with spherical particles with mean particle size of 154 μm and density 2485 kg/m^3. The superficial gas velocity is 0.133 m/s. Computational results are compared mutually, as well as against experimental data. The discrepancies are discussed.

INTRODUCTION

Fluidized beds are widely used in industrial operations, and several applications can be found in chemical, petroleum, pharmaceutical, biochemical and power generation industries. In a fluidized bed gas is passing upwards through a bed of particles supported on a distributor. Fluidized beds are applied in industry due to their large contact area between phases, which enhances chemical reactions, heat transfer and mass transfer. The efficiency of fluidized beds is highly dependent of flow behaviour and knowledge about flow behaviour is essentially for scaling, design and optimisation.

Gravity and drag are the most dominating terms in the solid phase momentum equation. The application of different drag models significantly impacted the flow of the solid phase by influencing the predicted bed expansion and the solid concentration in the dense phase regions of the bed. Researchers have shown that their models are sensitive to drag coefficient [1-4]. In general, the performance of most current models depends on the accuracy of the drag formulation.

A number of different drag models have been proposed in modelling of fluidized beds. Ergun [5] developed a drag model that was derived empirically for Newtonian flow through packed beds in a narrow band of porosities around 0.4. In an active fluidized bed the void fraction can vary over the whole range from zero to unity and the models used in numerical simulations should be equally versatile. Gidaspow [6] combined the Ergun equation with the equations of Rowe [7] and Wen and Yu [8] to get a drag model that can cover the whole range of void fractions. Gibilaro et al. [9] proposed a model for the friction coefficient that was included in the total gas/particle drag coefficient. This model is valid for the whole range of particle concentrations. Syamlal and O'Brian [10]

NOMENCLATURE

C_D	[-]	Friction coefficient
d_s	[m]	Particle diameter
e	[-]	Coefficient of restitution
g_i	[m/s^2]	Acceleration due to gravity
g_0		Radial distribution function
K_{qm}	[kg/m^3·s]	Coefficient for the interface force between the fluid phase and the solid phase
p	[Pa]	Fluid pressure
p_s	[Pa]	Solid phase pressure
Re_s	[-]	Particle Reynolds number
U_{qi}	[m/s]	Velocity vector for phase q
v_r	[m/s]	Terminal velocity

Special characters

α_q	[-]	Volume fraction of phase q
δ_{ij}	[-]	Kroenecker delta
ρ_q	[kg/m3]	Density of phase q
$\bar{\bar{\tau}}_{ij}$	[kg/m·s^2]	Stress tensor
μ	[kg/m·s]	Viscosity
ξ_s	[kg/m·s]	Bulk viscosity
Θ_s	[m^2/s^2]	Granular temperature

Subscripts

I, j, k	I, j and k directions
g	Gas phase
s	Solid phase

have also developed an empirical drag model that that can cover the whole range of void fractions.

The success of numerical computation of bubbling fluidized beds critically depends upon the ability to handle dense packing of solids. At high solid volume fraction, sustained contacts between particles occur and the resulting frictional stresses might be accounted for in the description of the solid phase stress. Granular flows can be classified into two flow regimes, a viscous regime and a plastic regime. In a viscous or rapidly shearing regime, the stresses arise because of collisional or translational transfer of momentum, whereas in a plastic or slowly shearing regime, the stresses arise because of Coulomb friction between grains in enduring contact [11].

In the present study the Eulerian approach is used to investigate gas-solid flow in a three dimensional fluidized bed. Gidaspow drag model and the drag model of Syamlal & O'Brien are the default drag models in Fluent 6.3, and the simulations in the present study are based on these two drag models. The frictional stresses are not included in the simulations.

PHYSICAL DESCRIPTION OF BED DYNAMICS

Computational studies have been performed on a 3-dimensional fluidized bed. Spherical particles with a mean diameter of 154 µm and a density of 2485 kg/m^3 are used. The behaviour of particles in fluidized beds depends on a combination of their mean particle size and density. Geldart fluidization diagram [12], shown in Figure 1, is used to identify characteristics associated with fluidization of powders. The current particles are classified as Geldart B particles, but are very close to Geldart A particles. The fluidization properties for these two groups of particles differ significantly from each other.

Particles characterized in group A are easily fluidized and the bed expands considerably before bubbles appear. This is due to inter-particle forces that are present in group A powders [13]. Inter-particle forces are due to particle wetness, electrostatic charges and van der Waals forces. Bubble formation will occur when the gas velocity exceeds the minimum bubble velocity and the bubbles rise faster than the gas percolating through the emulsion. For group B particles the inter-particle forces are negligible and bubbles are formed as the gas velocity reaches the minimum fluidization velocity. The bubble size increases with distance above the gas distributor and increases also with increasing excess gas. The bed expansion is small compared to group A particles.

NUMERICAL METHOD

The computational work is performed by using the commercial CFD code Fluent 6.3. The model is based on an Eulerian description of the gas and the particle phase. The default settings in Fluent 6.3 are used to describe the granular phase [14]. The energy equation is not solved, and it is assumed that there is no mass transfer between the phases.

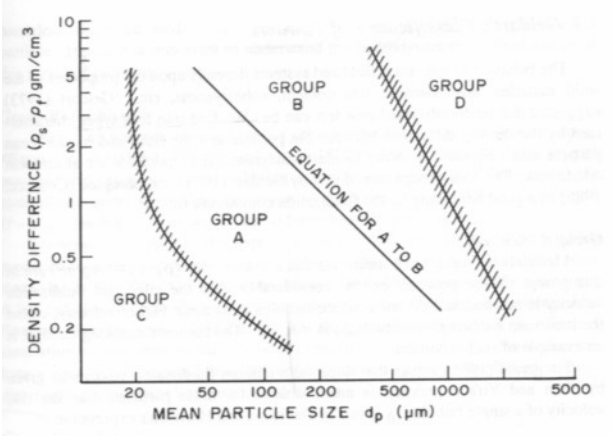

Figure 1 Geldart classification of particles according to their fluidization behaviour [12]

The continuity equation for phase q can then be expressed as:

$$\frac{\partial}{\partial t}\left(\alpha_q \rho_q\right)+\frac{\partial}{\partial x_i}\left(\alpha_q \rho_q U_{i,q}\right)=0 \tag{1}$$

The momentum equation in the j direction for phase q is:

$$\frac{\partial}{\partial t}\left(\alpha_q \rho_q U_{j,q}\right)+\frac{\partial}{\partial x_i}\left(\alpha_q \rho_q U_{i,q} U_{j,q}\right)= -\alpha_q \frac{\partial P}{\partial x_j}+\frac{\partial \bar{\tau}_{ij,q}}{\partial x_j}+\alpha_q \rho_q g_j+\sum_{m=1,m\neq q}^{M} K_{qm}\left(U_{j,m}-U_{j,q}\right) \tag{2}$$

where the terms on the lower line represent the pressure forces, viscous forces, mass forces and drag forces respectively. The gas phase stress tensor is expressed by:

$$\bar{\tau}_{ij,g}=\mu_g\left[\left(\frac{\partial U_{gj}}{\partial x_i}+\frac{\partial U_{gi}}{\partial x_j}\right)-\frac{2}{3}\delta_{ij}\left(\frac{\partial U_{gk}}{\partial x_k}\right)\right] \tag{3}$$

and the solid phase stress tensor is:

$$\bar{\tau}_{ij,s}=-p_s\delta_{ij}+\mu_s\left(\frac{\partial U_j}{\partial x_j}+\frac{\partial U_{si}}{\partial x_i}\right)_s+\left(\xi_s-\frac{2}{3}\mu_s\right)\delta_{ij}\left(\frac{\partial U_k}{\partial x_k}\right)_s \tag{4}$$

In the simulations the bulk viscosity is set to zero, and the solid viscosity is set constant. The solid phase pressure is modelled based on the kinetic theory of granular flow and is expressed by the following equation [14]:

$$p_s=\alpha_s\rho_s\Theta_s\left[1+2(1+e)g_0\alpha_s\right] \tag{5}$$

where the terms on the right hand side represent the kinetic and the collisional contribution to the solid pressure respectively. The radial distribution function expresses the probability of collisions between the particles. The function will approach unity for dilute regions and infinity in the dense regions of the bed. The radial distribution function is given by [15]:

$$g_0 = \left[1 - \left(\frac{\alpha_s}{\alpha_{s,\max}}\right)^{\frac{1}{3}}\right]^{-1} \quad (6)$$

In a bubbling fluidized bed the concentration of particles varies from very low to very high. In dilute regions, the kinetic of the particles will dominate the solids viscosity, and the solid pressure will be close to zero. In regions with higher concentration of particles, the collisions between particles will dominate the solids viscosity, and the solid pressure will increase. At very high concentration of particles, the frictional stresses dominate the solid viscosity. In this study the frictional stresses are not accounted for.

Drag models

The drag describes the momentum exchange between phases and is expressed by the drag coefficient K_{qm} in the momentum equation. In this work two different drag models are used, The Gidaspow drag model and the Syamlal & O'Brien drag model. The Gidaspow drag model is a combination of the Ergun equation and the drag model of Wen and Yu. The Ergun equation is developed for packed beds and is only valid at high particle concentrations. To get a model that covers the whole range of particle concentrations, the Wen and Yu equation is used for the lower concentrations. The Gidaspow model for gas particle drag is:

$$K_{sg} = 150\frac{\alpha_s(1-\alpha_g)\mu_g}{\alpha_g {d_s}^2} + 1.75\frac{\rho_g \alpha_g \left|\vec{U}_g - \vec{U}_s\right|}{d_s} \quad (7)$$

This is the Ergun equation and is valid for $\alpha_g \leq 0.8$. The Wen and Yu equation is valid for $\alpha_g > 0.8$, and is expressed by:

$$K_{sg} = C_D \frac{3\alpha_s \alpha_g \rho_g \left|\vec{U}_g - \vec{U}_s\right|}{4 d_s} \alpha_g^{-2.65} \quad (8)$$

The friction coefficient is developed by Rowe, and is related to the Reynolds number:

$$C_D = \frac{24}{\mathrm{Re}_s}\left(1 + 0.15\,\mathrm{Re}^{0.687}\right), \qquad \mathrm{Re} \leq 1000$$
$$C_D = 0.44, \qquad \mathrm{Re} > 1000 \quad (9)$$

The Syamlal & O'Brien drag model is:

$$K_{sg} = C_D \frac{3\alpha_s \alpha_g \rho_g \left|\vec{U}_g - \vec{U}_s\right|}{4 {v_r}^2 d_s} \quad (10)$$

The formula for the terminal velocity is developed by Garside and Al Dibuouni [14] and is an analytical formula:

$$v_r = 0.5\left(A - 0.06\,\mathrm{Re}_s + \sqrt{(0.06\,\mathrm{Re}_s)^2 + 0.12\,\mathrm{Re}_s(2B - A) + A^2}\right) \quad (11)$$

The constants A and B are:

$$A = \alpha_g^{4.14}$$
$$B = 0.8\alpha_g^{1.28}, \qquad \alpha_g \leq 0.85$$
$$B = \alpha_g^{2.65}, \qquad \alpha_g > 0.85 \quad (12)$$

The drag factor is proposed by Dalla Valle [14] and is expressed by:

$$C_D = \left(0.63 + \frac{4.8}{\sqrt{\mathrm{Re}_s / v_r}}\right)^2 \quad (13)$$

The granular temperature is a measurement for the random movement of the particles and influences on the solid pressure. In Fluent 6.3 there are two options for calculation of the granular temperature. The granular temperature can be described with a separate conservation equation or with an algebraic expression [14]. The algebraic expression is used in this work.

The governing equations are solved by a finite volume method, where the calculation domain is divided into a finite number of non-overlapping control volumes. The simulations are performed using three-dimensional Cartesian co-ordinates. The conservation equations are integrated in space and time. This integration is performed using first order upwind differencing in space and is fully implicit in time.

COMPUTATIONAL SET-UP

A computational study of bubble behaviour in a 3-D fluidized bed is performed. The cross section area of the bed is 0.25 m x 0.25 m and the height is 2.0 m. The initial particle height is 0.75 m, and the initial void fraction in the packed bed is 0.4. A three dimensional Cartesian co-ordinate system is used to describe the fluidized bed. The grid resolution is 10 mm in horizontal and vertical direction and the total number of control volumes is 125000. Spherical particles with a diameter of 154 μm and density 2485 kg/m^3 are used. The coefficient of restitution is set to 0.9. The boundary conditions are given as velocity inlet and pressure outlet. The inlet superficial gas velocity is set to 0.133 m/s and the outlet pressure is 1 atm. The simulations are run for about 20 s real time, and the computational results are compared to experimental data obtained on a corresponding fluidized bed with the same set-up and flow conditions. The calculated minimum fluidization velocity for particles with diameter of 154 μm and density 2485 kg/m^3 is 0.02 m/s [6], and according to Geldart fluidization diagram the particles are characterized as B particles.

RESULTS

The simulations are run with Syamlal & O'Brien drag model and with Gidaspow drag model. Figure 2 shows the mean void fraction as a function of radial position in the bed. The results are presented at height 0.39 m and 0.55 m. The results from the two drag models give no significant difference

in void fraction. Both models give lowest void fraction in the centre of the bed, and that indicates that the bubble frequency is lowest in this area. The variation in void fraction over the bed is about 0.01-0.04. Gidaspow at height 0.55 m gives the lowest variations and Gidaspow at height 0.39 m gives the highest variation.

The void fraction in the packed bed is 0.4, and according to the results shown in Figure 2, the mean void fraction in the fluidized bed is about 0.54. That means that the bed has expanded significantly, from initial bed height 0.75 m to a bed height of about 1.0 m. The mean bed height in the experimental fluidized bed was 0.85 m.

In this study the computational bubbles are defined as void fractions higher than 0.65. This definition is used because it was observed from the experimental study that parts of the bubbles can include high fractions of solids. Another reason for using a rather low void fraction in the definition of bubbles is that bubbles might occupy only a part of the control volume, and the mean void fraction for the control volume will then be lower than the void fraction in a bubble but higher than the mean void fraction in the bed. Figure 3 shows a plot of void fraction as a function of time at one position in the bed. It can be seen that the void fraction in this point varies from 0.4 to 0.77. The highest peaks represent the bubbles.

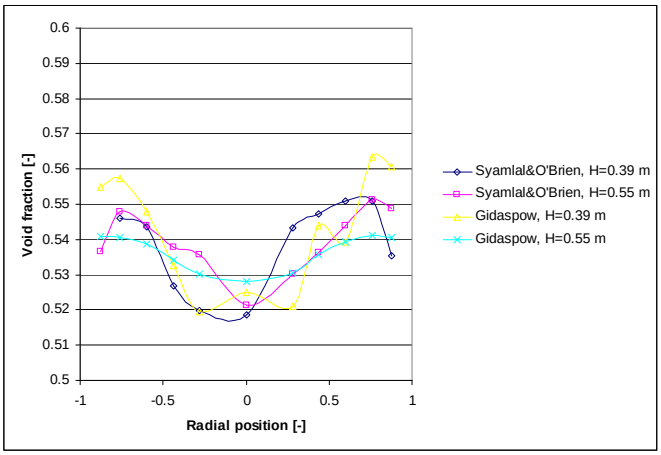

Figure 2 Void fractions as a function of radial position at different bed heights.

In Figure 4 a time series of solid volume fraction from the simulation with Syamlal & O'Brien drag model is presented. A bubble is assumed to be a region of void fraction greater than 0.80 [6]. The white areas in the fluidized bed represent void fractions greater than 0.8. It can be seen that very few bubbles satisfy this criterion. As the bed expands, the bubbles get smaller and more diffuse. After about 8 seconds the bed is stabilized at a high void fraction and only contours of small bubbles can be observed.

Figure 5 shows a comparison between the computational and experimental bubble frequency [16]. The experimental bubble frequency is significantly higher than the bubble frequencies obtained from the simulations. The Syamlal & O'Brien drag model gives slightly higher bubble frequency than the Gidaspow model.

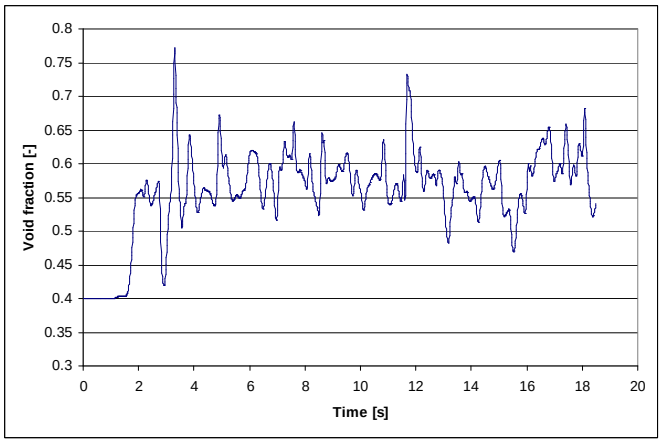

Figure 3 Bubble frequency as a function of time.

Discussion

Bubbling fluidized beds need rather long time to obtain quasi-steady state. In the experiment referred to in this work, the bubble frequency has been 1-3 bubbles per second. In the experimental study the bubble frequency was averaged over 20 minutes, whereas the computational results are averaged over 18-20 seconds due to long computational simulation time. This may explain the unsymmetrical computational void fraction profiles.

The low bubble frequencies in the simulations can be explained by the difference in the calculated and the experimental minimum fluidization velocity. The theoretical minimum fluidization velocity for spherical particles is given by:

$$U_{mf} = \frac{d_p{}^2 \Delta\rho \cdot g}{\mu} \cdot \frac{\alpha_{mf}{}^3}{1-\alpha_{mf}} \qquad (14)$$

where $\frac{\alpha_{mf}{}^3}{1-\alpha_{mf}}$ is approximately 11 [8] .

The theoretical minimum fluidization velocity for the current particles is 0.019 m/s, whereas in the experimental study, the observed minimum fluidization velocity was 0.07 m/s. In the experimental study, glass particles with a mean diameter of 154 μm were used. These particles have a particle size distribution that will influence on the flow conditions in the bed. This is not accounted for in the simulations. To account for the particle size distribution, the simulations can be run with multiple particle phases with different diameters. The particle size distribution in the experimental fluidized bed influences on the minimum fluidization velocity, and it was also observed that the particles behaved more like Geldart A particles, where the bed expands considerably before the bubbles appear. For group A particles bubbles appear as the gas velocity exceeds the minimum fluidization velocity, whereas for group B particles bubbles appear as the gas velocity reaches the minimum fluidization velocity.

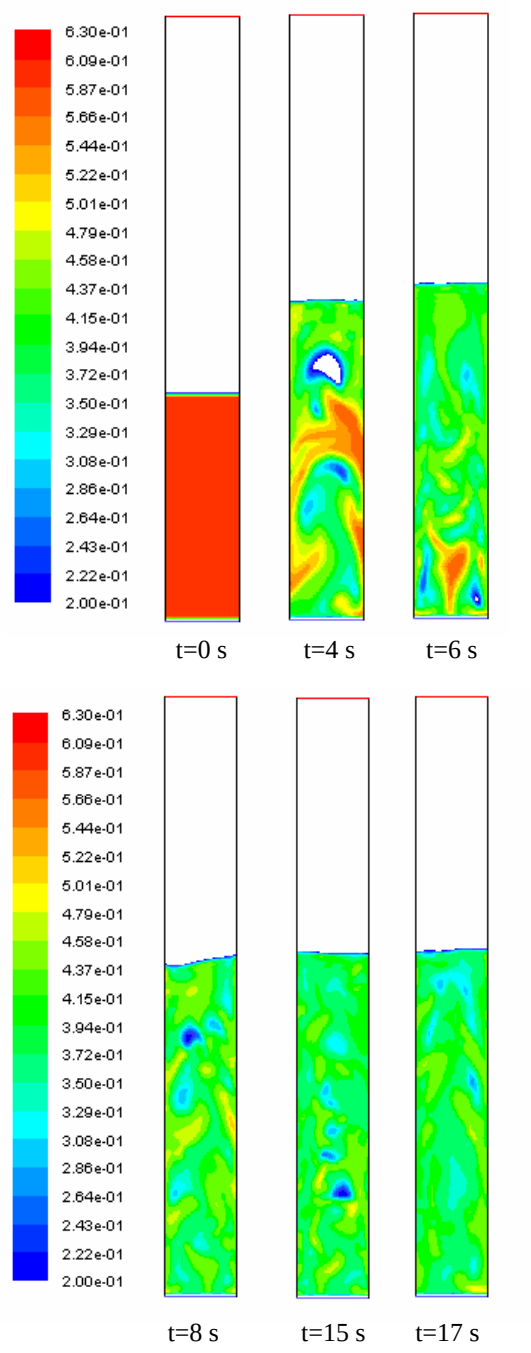

Figure 4 Volume fractions of solids. Syamlal & O'Brien drag model.

The excess gas velocity is defined as the difference between the superficial gas velocity and the minimum fluidization velocity. In the experiments, the ratio between the superficial gas velocity and the minimum fluidization velocity was about 2 whereas in the simulations this ratio is about 7. The high excess gas velocity, results in high bed expansion and thereby high mean void fraction in the bed. The conditions for bubble formations are then changed, and well defined bubbles may not appear.

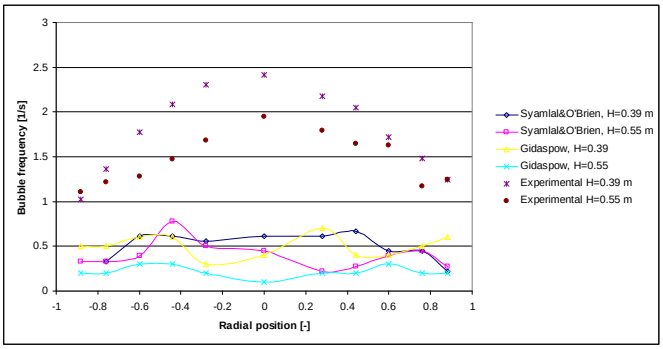

Figure 5 Bubble frequency as a function of radial position at different bed heights.

CONCLUSION

The CFD code Fluent 6.3 is used to study flow behaviour in a 3-dimensional bubbling fluidized bed. The Eulerian approach is used to describe the gas and the solid phase. The simulations are performed with Gidaspow drag model and the drag model developed by Syamlal & O'Brian. The results from the simulations with these two drag models do not differ significantly from each other. Both the models give high bed expansion, and a rather low bubble frequency. The bed expands from 0.75 m to about 1.0 m, and the bubble frequencies are about 0.5 s^{-1}. Well defined bubbles, that means a region of void fraction greater than 0.80, are only observed in the first 4 seconds. The Syamlal & O'Brian drag model gives slightly higher bubble frequency than the Gidaspow drag model.

The simulations are compared to experimental results. The experimental study is performed with spherical glass particles with mean particle size of 154 μm and density 2485 kg/m^3. The initial particle height is 0.75 m and the superficial gas velocity is 0.133 m/s. The same conditions are used for the simulations. In the experiments, however, the particles have a size distribution that covers particle sizes from about 50 μm to 250 μm. In the simulation all the particles are defined with the same diameter, 154 μm. The simulations give considerably lower bubble frequencies than the experiments. The experimental bubble frequency is about2 s^{-1}, and that is about 4 times the bubble frequencies obtained in the simulations. The bed expansion in the experiments is about 0.1 m, whereas it is about 0.25 m in the simulations. The discrepancies between computational and experimental result may be due to the different ranges of particle sizes. The observed experimental minimum fluidization velocity is about 4 times the calculated minimum fluidization velocity for particles with diameter 154 μm. The consequence of this is that the excess gas velocity becomes much higher in the simulations than in the experiments, and the ideal conditions for a bubbling fluidized bed might no longer be present. To get a better agreement between simulations and experiments, the simulations should be performed with multiple particle phases to account for the particle size distribution in the experiments.

REFERENCES

[1] Yasuna, J.A., Moyer, H.R., Elliott, S., Sinclair, J.L. (1995), Qantitative predictions of gas-particle flow in vertical pipe with particle-particle interactions, *Powder Technology* **84**, pp. 23-34.

[2] Halvorsen, B., Mathiesen, V. (2002), CFD Modelling and simulation of a lab-scale Fluidised Bed, *Modeling, Identification and Control*, **23**(2), pp. 117-133.

[3] Ibsen, C.H. (2002), An experimental and Computational Study of Gas-Particle Flow in Fuidised Reactors, Ph.D. Thesis, Aalborg University, Esbjerg.

[4] Bokkers, G.A., van Sint Annaland, M., Kuipers, J.A.M. (2004), Mixing and segregation in a bidiperse gas-solid fluidised bed: a numerical and experimental study, *Powder Technology*, **140**, pp. 176-186.

[5] Ergun, S. (1952), Fluid Flow Through Packed Columns, *Chemical Engineering Progress*, **48**(2), pp. 89-94.

[6] Gidaspow, D. (1994), Multiphase Flow and Fluidization. Academic Press, Boston

[7] Rowe, P.N. (1961), Drag Forces in a Hydraulic Model of Fluidized Bed-PartII, *Trans. Instn. Chem*., **39**, pp. 175-180.

[8] Wen, C.Y., Yu, Y.H. (1966), Mechanics of Fluidization, *Chemical Engineering Progress*, **62**, pp. 100-111.

[9] Gibilaro, L.G., Di Felice, R., Waldram, S.P. (1985), Generalized Friction Factor and Drag Coefficient for Fluid-Particle Interaction, *Chemical Engineering Science*, **40(10)**, pp. 1817-1823.

[10] Syamlal, M., O'Brien, T.J. (1987), A Generalized Drag Correlation for Multiparticle Systems, Morgantown Energy Technology Center, DOE Report.

[11] Jenkins, J.T., Cowin, S.C. (1979), Theories for Flowing Granular Materials, Mech. Applied to Transport of Bulk Materials, *Ap. Mech.Div. of ASME*, 31, pp. 79-89.

[12] Geldart, D. (1973), Types of Gas Fluidization, *Powder Technology*, 7, pp 285-295.

[13] Geldart, D. (1986), Gas Fluidization Technology, John Wiley & Sons Ltd.

[14] Fluent, Fluent 6.2 Users Guide, *Fluent Inc., Lebanon, NH, USA*, 2005.

[15] Bagnold, R.A. (1954), Experiments on a Gravity-Free Dispersion of Large Solid Spheres in a Newtonian Fluid Under Shear. *Proc. of Roy. Soc.*, **A225**, pp. 49-63.

[16] Halvorsen, B., An experimental and computational study of flow behaviour in bubbling fluidized beds, Doctoral Thesis at NTNU: 70, 2005.

Appendix E

Abstract for the SIMS2008 conference in Oslo, Norway

A review of some existing drag models describing the interaction between phases in a bubbling fluidized bed

Joachim Lundberg[a], Britt M. Halvorsen[a,b], Vidar Mathiesen[c]
a. Telemark University College, Norway
b. Telemark Technological R&D Centre (Tel-Tek), Norway
c. StatoilHydro, Norway
E-mail: 023374@student.hit.no

This work represents a computational study of flow behaviour in a bubbling fluidized bed. The simulations are performed by using the commercial computational fluid dynamic (CFD) code, Fluent 6.3. The advantage of using a commercial CFD code is that corresponding cases for industrial applications can be simulated by using the same model without having very deep knowledge about the source code and the solving algorithms. In CFD simulations of fluidized beds, it is important to describe the interaction between the particles and the momentum transfer between the phases. Different models are developed for this purpose. The kinetic theory of granular flow describes the interaction between particles and is based on the kinetic gas theory. In a bubbling fluidized bed there are regions with rather low fraction of particles and regions with high particle concentrations, and the bed can be described by two flow regimes, the viscous regime and the frictional regime. In the viscous regime the kinetic and the collisional stresses are dominating. The frictional regime occurs at high particle concentrations and in this regime the flow behaviour is described by friction and rubbing between particles.

The interaction between the particles and the continuous gas phase are described by a drag model, and several drag models are developed for this purpose. The models describe the momentum exchange between the phases. The aim of this work is to study how the different drag models influence on the flow behaviour in a bubbling fluidized bed. Five different drag models have been studied. The drag models are the Gidaspow drag model, a drag model developed by Syamlal & O'Brien, a customized iterative version of the drag model by Syamlal & O'Brien, the modified Hill-Koch-Ladd drag model and the newly developed RUC drag model. Two of the drag models are included in Fluent, and the other models are implemented by the author. The results from the simulations with the different drag models are compared, and the discrepancies are discussed.